Technical Report

A Systems Study of Fiber Optics for Broadband Communications

Activity No. 10
Wavelength Division Multiplexing

BNR Project TR 6259
March 1978

Bell-Northern Research

A Systems Study of Fiber Optics for Broadband Communications

BNR Project TR6259
March 1978

for
Communications Research Centre
Department of Communications
Government of Canada

under DSS Contract
File number: 12ST. 36001-6-2350
Contract number: OST 76-00054

Activity No. 10
Wavelength Division Multiplexing

J. Straus
P. Pierroz
M. Larose

Bell-Northern Research Ltd.

TABLE OF CONTENTS

Acknowledgements

The authors are grateful to J. Conradi, F.P. Kapron, and J.C. Dyment for their comments on the manuscript. The authors also acknowledge N. Toms for his contribution to this report, especially to Section 6.

LIST OF TABLES

LIST OF FIGURES

LIST OF FIGURES (Cont'd)

1. INTRODUCTION

This report is the tenth and last Activity report of the Systems Study of Fiber Optics for Broadband Communications undertaken by Bell-Northern Research for the Canadian government's Department of Communications (DOC). This Activity report on wavelength division multiplexing replaces essentially the field trial definition activity that was planned in the initial study work outline. The scope of this latter activity has been expanded and it is now performed under separate government contracts.

In Activity reports no. 2,3 and 4 on the methodologies of using fiber optics for CATV, Asymmetric Interactive Switched Visual Services, and Integrated Distribution of Video, Voice and Data, Wavelength Division Multiplexing (WDM) is identified as a promising technique for multiplexing many channels on a single fiber. The report studies in further details the technical feasibility and limitations of WDM.

The sections of this report have been written by different authors. Therefore changes in style and some slight duplication of the materials are inevitable. However these are not believed to be detrimental to the comprehension of the report. Section 3 treats the system applications of WDM. It has been written by M. Larose with the collaboration of J. Straus. Section 4 deals with the properties of fibers, sources, and detectors as they relate to WDM. In Section 5 various methods of multiplexing and demultiplexing WDM signals are described. The principles and the performances of experimental multiplexers and demultiplexers are reviewed. Both Sections 4 and 5 have been written by J. Straus. In Section 6 the performance of a diffraction grating demultiplexer is analyzed in terms of the number of channels that can be demultiplexed, taking into account the dispersivity of the grating and lens aberrations. This section has been written by P. Pierroz.

2. SUMMARY AND CONCLUSION

The advantage of WDM systems, is that it permits multichannel signal operation without incurring the performance limitation of optoelectronic components which otherwise might occur in high level FDM systems. WDM is economically attractive over FDM for trunk line application when the number of channels multiplexed limit FDM to short repeater spacings. It is also attractive for subscriber line application when the use of FDM would require expensive linearization circuitry or when the WDM signal format is more adapted to the subscriber's equipment.

The most effective use of WDM will occur in the two low loss wavelength regimes of optical fibers. The 0.8-0.9 μm wavelength range is compatible with the presently available technology of GaAlAs light sources and Si detectors. The 1.0-1.3 μm regime has the advantage of reduced dispersion.

The majority of WDM systems will employ multimode graded index fibers as the transmission medium. The fabrication of this type of fibers is well established and attenuation figures as low as 2 dB in the 0.8-0.9 μm and 0.5-1 dB in the 1.0-1.3 μm range have already been attained respectively.

The choice of light sources for WDM applications will depend on several system parameters such as the operating wavelength range, number of channels transmitted, required signal-to-noise ratio and crosstalk. For immediate system needs, GaAlAs double heterostructure LED's and Fabry-Perot lasers emitting in the 0.8-0.9 μm regime can be used.

Distributed feedback (DFB) and distributed Bragg reflector (DBR) lasers are especially attractive for WDM applications due to their high wavelength selectivity, narrow spectral width and minimal temperature dependence of the emission wavelength. Presently however, the efficiency of DFB lasers is only 10-20% that of Fabry-Perot devices and their reliability is not yet established. Furthermore they eliminate the need for Fabry-Perot mirrors which are incompatible with monolithic device integration. Integrated DFB lasers emitting at several different wavelengths, with outputs coupled into a common waveguide have been fabricated. These devices are particularly suitable for WDM applications.

For longer wavelength operation light sources fabricated from ternary and quaternary alloys of III-V compounds will be used. Although the technology of longer wavelength devices is still at an early stage the results so far obtained indicate that performances comparable to those of GaAlAs devices can be obtained.

As far as the number of transmitted channels is concerned LED's due to their wide spectral width will not permit more than 3-5 channels to be multiplexed into the 0.8-0.9 μm or 1.0-1.3 μm wavelength range. It is anticipated that integrated DFB lasers will permit as many as 10 channels to be multiplexed into a 20 nm wavelength interval. Staggered multiplexing of several integrated DFB lasers chips could lead to systems with 20-30 channels. The performance of such a system will be limited by the internal multiplexing efficiency between the separately integrated elements. With 10 nm wavelength spacing for Fabry-Perot lasers, 10 channels at least, could be multiplexed into a 100 nm wide spectral band. The exact number of channels will depend both on crosstalk and signal-to-noise ratio considerations.

Designs of WDM systems should also take into account the influence of temperature, of drive currents and of aging on spectral properties of light sources. Device heating, can lead to emission wavelength shifts towards longer wavelengths while aging and modulation currents can lead to increased spectral broadening. These in turn will result in an increased crosstalk and insertion loss.

In reference to detectors, Si PIN's and avalanche (APD) photodiodes can be used in the 0.8-0.9 μm regime. The choice between the two detectors will depend on the transmission rate and the required system sensitivity. For shot noise limited systems Si PIN's are adequate. For systems limited by preamplifier noise APD's will be preferred. In the 1.0-1.1 μm regime specially developed side entry Si detectors can be used. These devices will compete with detectors fabricated from Ge or alloys of III-V compounds. As far as excess noise is concerned Si detectors have the advantage. For immediate applications beyond 1.1 μm Ge detectors are commercially available. Future systems in the 1.0-1.3 μm wavelength range will most likely use recently developed photodetectors made of alloys of III-V compounds. The advantage of this type of detectors is that their response can be tailored specifically for each given wavelength range. Integrated photodetectors based on electroabsorption effects have also been proposed. This type of detector is particularly suitable for efficient demultiplexing of optical signals. Their implementation however remains to be demonstrated.

The results of the study indicate that there are no major conceptual difficulties which could limit the development and the fabrication of multiplexers and demultiplexers for WDM system applications. Nondispersive (coupler-like), dispersive (gratings, prisms) elements as well as elements based on wavelength dependent reflectivity and transmission (interference filters, holographic grating) have been considered for multiplexing of optical signals. Devices based on the latter two effects (dispersive and interference based) are also suitable for the more demanding role of demultiplexers.

In systems with relatively low number of channels (~2-5) the use of coupler like elements is preferred for optical multiplexing. The devices have low insertion loss and are relatively easy to fabricate. Two typical representatives of this type of devices are the multifiber combiner (~ 1 dB insertion loss for 3 channels) and the GRIN rod lens based multiplexer (~ 3 dB loss for a 4 channel system). The advantage of a multifiber combiner is that it eliminates the need for a focusing optics between the light source and the multiplexer. The insertion loss of coupler like multiplexers in systems containing a large number of channels (10-20) increases rapidly and improved multiplexing techniques are mandatory. The use of diffraction gratings and prisms provides the necessary solution. These two devices are also suitable and in fact, preferred for optical demultiplexing. The efficiency of blazed plane diffraction grating can be as high as 75-90% over the entire spectral range of interest. Insertion losses of at least 5-7 dB for systems containing 10-30 channels, however, are more realistic. Immersed designs in forms of epoxies between the collimator and the demultiplexer offer an advantage in increased ruggedness and reduced crosstalk and system losses. The effect of grating imperfections needs also to be considered.

The insertion loss of prisms in experimental WDM systems presently is about 3 dB. Theoretical considerations indicate that an insertion loss of 1 dB for low number of multiplexing channels should be attainable. The choice of prism material will depend on the wavelength range of operation. CdS and $Ga_{0.8}Al_{0.2}As$ are suggested for the 0.7-0.87 µm band while SiO_2, CdS, CdSe and $Ga_{0.9}Al_{0.1}As$ are to be used for 2 0.9 multiplexing the 0.85 - 1.05 µm band. There are currently no adequate materials available for the operation near the 1.3 µm regime. Epoxies could also be used for prism multiplexers to ensure mechanical stability.

The use of demultiplexers based on interference effects in near future will be limited to systems with no more than 2-3 multiplexed channels. The main reason for this conclusion is due to the lack of available materials and technology which would permit the fabrication of low loss demultiplexing devices in systems containing larger number of channels. Future developments however could rectify this situation. On this basis, multiple thick reflection grating devices (chirped gratings) offer a promise due to their compactness and potential for optical integration.

A practical design of a WDM system using a diffraction grating as the demultiplexing element is considered in section 6. The results of calculations indicate the possibility of demultiplexing seven channels within the 0.8-0.9 µm wavelength band using lasers as light sources and assuming 60 dB electrical crosstalk between the adjacent channels. The insertion loss of the demultiplexer is estimated 3 dB. The number of multiplexed channels for the given crosstalk in this example is limited by the aberration of optical elements in the system. This number could further be reduced due to variations of spectral properties of lasers with temperature, modulation, and aging.

In conclusion, the results of considerations indicate that there are no significant impediments which could limit the development of practical WDM systems in the future. Further experimental work is required to assess the feasibility, performance, and, consequently, cost attractiveness of practical WDM systems.

3. SYSTEM CONSIDERATIONS

3.1 APPLICATION AREAS

In the Activity Reports no. 2, 3 and 4 of this study, Wavelength Division Multiplexing (WDM) is identified as being an attractive multiplexing technique. It is considered for application in trunks, feeder, and drop in a non-switched tree structure CATV system. It is also considered for trunks and subscriber lines in a switched system which provides CATV, asymmetric visual services or the integrated distribution of video, data, and telephony. The need for high level of multiplexing on trunks is especially acute in low population density rural areas. In the switched systems considered, the uni-fiber subscriber line is used for both downstream and upstream transmissions. WDM could prevent amplifier saturation caused by accidental high power near end light reflection, if the optical signals received by the detector are segregated with respect to their wavelength.

WDM is considered mainly because it could circumvent the source power and linearity limitations associated presently with frequency division multiplexing (FDM). WDM could also represent advantages in terms of fiber bandwidth, especially in repeatered lines where the use of WDM could alleviate the need for fiber equalizers. These are likely to be required in multi-channel FDM systems due to the repeater cascade effect.

On the aspect of the overall system, WDM could achieve longer transmission lengths and wider repeater spacings. In a non-switched tree structure network using optical tapping, it could permit the realization of longer feeder sections, as compared with FDM systems. However WDM has the disadvantage of requiring more sources, detectors, and amplifier modules, than FDM. This problem is more significant in repeatered trunk lines because demultiplexing, individual amplification of the channels, and remultiplexing are required at each repeater. The cost of WDM terminals is likely to be higher than for FDM. The complexity of the multiplexer and demultiplexer is also an unknown.

The pros and cons of WDM systems are very dependent on their performance in terms a) the power per channel that would be coupled in a fiber and received at the other end by the corresponding detector; b) the number of channels that could be multiplexed and demultiplexed while meeting the signal-to-noise ratio and isolation requirements. These, in turn, are influenced by factors such as performance and availability of adequate light sources, feasibility and efficiency of mux-demux. These aspects are studied in Sections 4, 5 and 6.

3.2 ECONOMIC CONSIDERATIONS

In this section the economic trade-offs between FDM and WDM are addressed. There are basically two situations: 1-in repeatered trunk lines where the increase in repeater spacing for WDM could counterbalance the higher repeater unit cost; 2-in subscriber lines where WDM could represent a cheaper multiplexing scheme.

3.2.1 Trunk Lines

The economic trade-off between WDM and FDM for repeatered trunk lines can be expressed as follows:

$$\frac{\text{WDM repeater cost}}{\text{WDM repeater spacing}} \quad \overset{?}{\lessgtr} \quad \frac{\text{FDM repeater cost}}{\text{FDM repeater spacing}}$$

The WDM repeaters are likely to be more than 1.5 times more expensive than FDM repeaters because they require a MUX-DEMUX and more sources, detectors, and amplifier modules. Although FDM repeaters require wider bandwidth and more linear amplifiers, the cost of these is expected to follow a N^x trend, as opposed to a N trend expected for WDM repeaters, where N is the number of channels and x is smaller than one for FDM. Therefore the amplification circuitry for WDM repeaters would contribute to make them significantly more expensive than FDM repeaters.

For a low number of channels, (e.g. 5 channels) the increase in repeater spacing that could result from the use of WDM would not be sufficient to make WDM systems economically attractive over FDM systems. For higher number of channels (e.g. 12 channels), FDM systems are limited to short repeater spacings due to power and linearity limitations. WDM systems could be economically attractive if the same number of channels can be multiplexed, the crosstalk requirement be met, and if the MUX-DEMUX insertion loss does not increase significantly with the number of channels multiplexed.

3.2.2 Subscriber line

The subscriber line in a switched system involves a lower level of multiplexing than the one required for trunk lines. The multiplexing of up to three video channels, plus possibly, some data and telephony channels might be required in this case. The economic trade-off between FDM and WDM for subscriber line application can be expressed as follows:

$$\begin{array}{c} \text{WDM cost of RSU interface} \\ \text{unit + subscriber terminal} \end{array} \quad \overset{?}{\lessgtr} \quad \begin{array}{c} \text{FDM cost of RSU interface} \\ \text{unit + subscriber terminal} \end{array}$$

The interface unit at the remote switching unit (RSU) assumes the interface between the subscriber fiber line and the different switches (e.g. video, telephony and data switches). It performs the multiplexing and electro-optic conversion of the different channels. The subscriber terminal assumes the interface between the subscriber fiber line and the subscriber's equipment (e.g. TV, telephone, and data sets).

The cost trade-off is really between the FDM multiplexing circuitry and the supplementary light sources and detectors, amplifiers, and mux-demux required for WDM. Partial lists of components required by the two multiplexing techniques for a switched CATV system providing each subscriber with three different video channels are given below for comparison, presently available TV sets are assumed.

WDM	FDM
4 light sources + driving circuitries	2 light sources + driving circuitries
4 PIN + amplifiers	2 PIN + amplifiers
3 frequency converters	3 frequency converters
2 MUX-DEMUX	FILTERS

The items omitted in the above list, either are common to both approaches or do not have a significant cost impact on the interface unit or the subscriber terminal. The video switching is assumed to be done at a low RF channel (e.g. T7). Therefore frequency converters can be used. The filters required by the FDM approach do not have strict transmission performance requirements associated with them, hence they are believed to be much less expensive than the two MUX-DEMUX. From the above list of components it can be concluded that the WDM approach is likely to be more expensive than the FDM approach. However the conclusion could be different if source linearization circuitry was required for the FDM transmission on this limited number of channels, or if future sets accept baseband or low RF signals. In the latter case the three frequency converters would not be required in the WDM subscriber terminal and it would permit significant cost savings.

4.0 COMPONENTS FOR WDM SYSTEMS

4.1 INTRODUCTION

In this chapter the review of the present state-of-the-art of basic optoelectronic components is made with an emphasis on WDM system applications. The expected trends in developments towards components for longer wavelength (1.0-1.3 μm) application are also discussed. Besides increased spectral range beyond the available 0.8-0.9 μm regime in WDM systems the rationale for longer wavelength components arises because of decreased attenuation and pulse broadening in fibers. An analysis of system considerations for longer wavelength regimes has been given recently.[1,2] The results confirm the superiority of systems operating at longer wavelengths. It is expected that future WDM systems will also utilize the advantage of this mode of operation.

This section is divided into 5 parts. Section 4.2 treats fibers, section 4.3 light sources, section 4.4 detectors. A summary of these three sections is presented in section 4.5

4.2 FIBERS

It appears presently that the majority of WDM systems will employ multimode rather than single mode fibers. The advantage of multimode fibers is in their proven fabrication technology and in the relative ease of their handling in coupling, splicing and connectorization. The importance of single mode fibers will increase with requirements for systems with high transmission rate capacity.

The following fiber parameters are of prime importance: attenuation vs. wavelength λ, pulse broadening and coupling efficiency of radiation into fiber. The influence of these parameters on WDM system design is discussed below.

4.2.1 Attenuation

Recent improvements in fiber manufacturing technology have yielded fibers with attenuation as low as 3 dB in the 0.8 - 0.9 μm wavelength range,[3] the range of presently available light sources and detectors. The attenuation decreases to between 0.5 and 1 dB/km in the 1.0-1.35 μm wavelength range, depending upon the silica dopant, very close to the intrinsic scattering limit. The loss figures are quite susceptible to dopant profile variations, to spatial variations in fiber geometry, to microbending as well as gross bending.

4.2.2 Pulse Broadening

The two major factors contributing to pulse broadening are material and multimode dispersion. Material dispersion is caused by the wavelength dependence of the index of refraction as a result of which several wavelength components of a pulse will propagate through the fiber with different time delays. For a light source with a spectral width $\Delta\lambda$, the pulse broadening Δt in a fiber length L is equal to

$$\frac{\Delta t}{L} = \frac{1}{c} \left(\frac{\Delta\lambda}{\lambda}\right) \lambda^2 \frac{d^2 n}{d\lambda^2}$$

where n denotes the index of refraction and c the speed of light.

In general, $\frac{d^2 n}{d\lambda^2}$ decreases towards longer wavelengths with a minimum occurring near 1.3 μm and then increases again. The fact that $\frac{d^2 n}{d\lambda^2}$ decreases with wavelength suggests that a device in the 1.0 - 1.3 μm wavelength range is superior to a device emitting at 0.8 μm as far as pulse broadening is concerned.[4] As an illustration, the estimated pulse broadening for LED's with $\Delta\lambda = 40$ nm at $\lambda = 800$ nm,

is $\Delta t/L = 4.2$ ns/km. However, for a source emitting at 1.1 μm with the same $(\Delta\lambda/\lambda)$ the pulse broadening is only $\Delta t/L = 0.9$ ns/km, a considerable reduction.

Multimode dispersion is due to transmit time differences between various propagation modes of the waveguide. The multimode dispersion in step index fibers is of the order of

$$\frac{\Delta t}{L} \simeq \frac{\Delta n}{c}$$

with Δn denoting the core-cladding index of refraction difference. For $\Delta n = 0.015$, $\Delta t/L = 50$ ns/km. If mode mixing is present the pulse width increases with fiber length as $L^{0.5}$ rather than $L^{1.0}$ and reduced overall pulse broadening is obtained.[5]

Multimode dispersion in ideally graded index fibers is equal to:

$$\frac{\Delta t}{L} = \frac{(\Delta n)^2}{8cn}$$

with n denoting the mean index of refraction of cladding. For $\Delta n = 0.015$, $n = 1.5$, $\Delta t/L = 0.06$ ns/km which is much lower than that calculated for step index fibers with the same Δn. Mode coupling further reduces the value of pulse dispersion in a manner similar to that for step index fibers. To date values as low as 0.2 ns/km have been realized.[6]

It should be noted that multimode dispersion is slightly wavelength dependent, because of the dependence of the refractive index of glass constituents on wavelength. This and the accuracy sensitivity of the optimum profile has so far prevented attainment of the theoretically minimum value.

4.2.3 Coupling

Coupling from source to fiber, fiber-to-fiber and fiber-to-detectors is only weakly wavelength dependent and will not be further considered. A more critical figure of merit is the efficiency by which a fiber will accept radiation from a given source. This coupling efficiency is determined by the core diameter of the fiber, numerical aperture and index profile. The coupling efficiency of fibers varies roughly as $\approx(NA)^2$ and depends also on radiation pattern of the source. Typical coupling efficiency, into step index fiber NA = 0.14 is about -3dB, for a laser and about -10 to -17 dB for LED's depending on the device geometry.[7] A reduction of 2 to 3 dB in coupling efficiency is expected for graded index fibers.

4.3 SOURCES

In this section light sources which are potential candidates for applications in WDM systems are discussed. The different source types and geometries are considered in conjunction with those specific device properties which will directly influence the system configuration and performance.

The parameters of prime importance are: the available spectral range, the spectral stability and the spectral width. Additional device parameters such as power output, bandwidth and reliability also have to be considered. In analog applications device linearity must also be taken into account.

4.3.1 Materials For Different Emission Wavelength

To date various classes of light sources compatible with the two low loss regimes of optical fibers have been developed. These are listed in Table 4.1 and include LED's, lasers, and Nd:YAG crystals pumped by LED's.[1] Nd:YAG lasers cannot be fabricated in a wide wavelength range, they are relatively inefficient and require external modulation. Therefore it is expected that they will not be important in practical WDM systems and they will not be further considered.

The two wavelength regimes can be covered by light sources fabricated from III-V binary compounds and their ternary and quaternary alloys. The emission wavelength of a binary compound is basically determined by the bandgap of the material and consequently cannot be varied. By combining two binary compounds however, the resulting ternary has a bandgap value and lattice constant that is a function of the alloy composition.

Table 4.1 Summary of Materials for Light Sources
Emitting in the 0.8-1.3 μm Wavelength Range

LIGHT SOURCE	λ = 0.8-0.9 μm	1.0-1.1 μm	> 1.3 μm
LED's	GaAs/GaAlAs	GaInAs GaInAsP/InP GaAsSb	InGaAsP/InP
Injection Lasers	GaAs/GaAlAs GaAs/InGaP	InGaAs/InGaP InGaAsP/InP GaAsSb/GaAlAsSb	GaInAsP/InP
YAG/LED	–	Nd:YAG fibers	Nd:YAG fibers

For LED's and lasers, heterojunctions have been designated with two materials separated by an inclined line. Active layer is on left of line while confining layer is on right.

As a result, the emission wavelength of the alloy can be varied continuously over the entire range between the values for the binary compound forming the alloy. The wavelength range covered by eight of the more widely used III-V ternary alloys is shown in Figure 4.1.[8] The cross-hatched areas represent alloy compositions for which the energy gap of the alloy is direct, a requirement for high efficiency light generation.

The choice of materials for a required emission wavelength will depend on several parameters such as ease of fabrication, carrier mobility and most importantly lattice matching, particularly in heterostructure devices with adjoining epitaxial layers of dissimilar materials. As a cardinal rule it can be stated that the lattice constant of heterostructure devices must be matched as closely as possible. The development of AlGaAs heterojunction lasers and LED's in the 0.8 - 0.9 μm range, in fact, is the consequence of close lattice matching within the alloy system. The problem of lattice matching in ternary compounds for longer wavelength operation (GaInAs, GaAsSb, etc.) is slightly more difficult because of the difference between the lattice constants of the ternary and of the binary substrate. There are two techniques by which lattice matching in such situations is achieved. The first uses linear compositional grading between the substrate and the epilayer of the device while the other employs step grading. Both techniques are described in detail in Reference 8.

The disadvantage of compositional grading in longer wavelength ternaries is eliminated by using quaternary alloys. These materials have an additional degree of freedom in that they allow independent control of energy bandgap (i.e. of emission wavelength) and of lattice constant over wide ranges. The use of quaternary alloys in fabrication of photodetectors,[9,10] LED's[11,12] and room temperature CW operating lasers[13,14,15] has been reported recently.

In concluding this section it appears that there are no conceptual difficulties in fabricating light sources with different emission wavelengths. While GaAlAs technology in the 0.8 - 0.9 μm wavelength range is already well established the use of ternaries and quaternaries for preparation of longer wavelength devices is still at an early stage. The results attained however are extremely encouraging with performance levels close to (if not above) that of GaAlAs devices. As a result of these rapid developments it can be expected that the long wavelength devices in addition to presently available GaAlAs light sources will play an important role in the development and utilization of practical WDM systems.

4.3.2 Device Geometry and Configurations

Double heterostructure LED's are available as either top or side emitters. The light emission in top emitting LED's, is perpendicular to the junction plane while the emission in side emitters is parallel to the

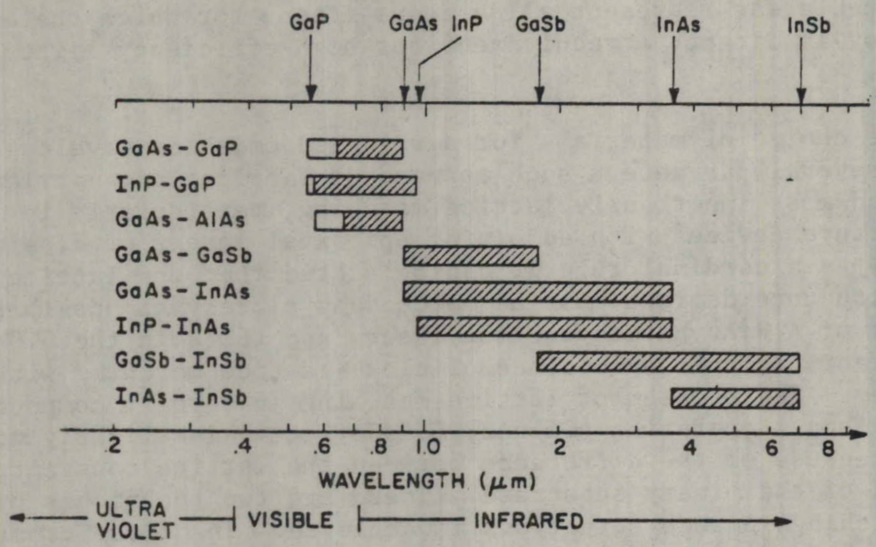

Figure 4.1 Room-temperature wavelength range covered by several commonly used III-V ternary alloys

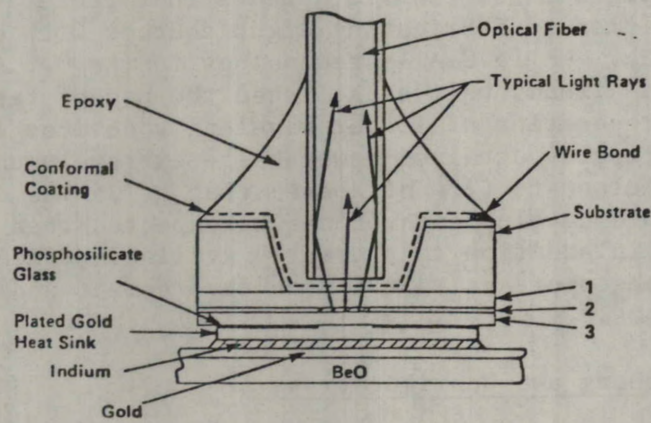

Figure 4.2 Double heterostructure top emitting Burrus LED. Layer 2 is the active layer while layers 1 and 3 are wider bandgap confining layers.

junction plane. A Burrus[16] type LED is a typical representative of a top emitter[17] (Figure 4.2). The geometry of side emitters[7] is similar to that of double heterostructure lasers (Figure 4.3).

A considerable interest also exists in the development of integrated optical devices, particularly in the fabrication of distributed feedback[18] (DFB) and distributed Bragg reflector[19] (DBR) lasers. (see Figures 4.4 and 4.5). A DFB (and DBR) laser is fabricated similarly to the standard Fabry-Perot type structures with the exception that the lasing action is obtained by the addition of periodic spatial variation of the refractive index within or adjacent to the gain medium of the laser. The feedback in the cavity occurs because the energy of a wave propagated in one direction is continuously fed back in the opposite direction by Bragg scattering. The advantage of these devices is that they eliminate the need for Fabry-Perot mirrors which are imcompatible with monolithic device integration. Further advantages of DFB lasers stem from high wavelength selectivity and narrow spectral width and minimal temperature dependence of emission wavelength. The properties DBR lasers are similar to that of DFB lasers and will not be discussed separately.

Because of the relatively early stage of integrated optics technology most of the immediate research in this area is expected to remain concentrated on GaAlAs type materials. As the advantages of fiber optics at longer wavelengths become more established the development of other materials for integrated optics will follow.

4.3.3 Properties of LED's and Lasers

Table 4.2 summarizes the typical properties of LED's and lasers which might be considered in WDM systems applications. In the following these are described with an emphasis on wavelength related characteristics.

a) Spectral Properties

1- Peak Wavelength

As mentioned in the previous section the peak wavelength of LED's and lasers will be determined by the alloy composition of the active layer. The emission wavelength also depends on the type and the amount of dopant in the active layer of the device. The effect is attributed to the existence of radiative recombination centers within the bandgap of the active material and can result in wavelength shifts which are on the order of 10-15 nm.

The following relationship connects the emission wavelength λ of DFB lasers to the grating period Λ and grating order m:

$$\Lambda = \frac{\lambda m}{2n}$$

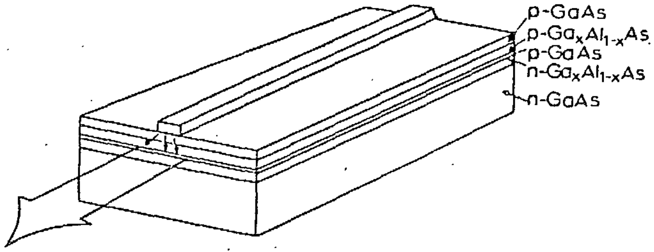

Figure 4.3 Double-heterostructure stripe geometry laser

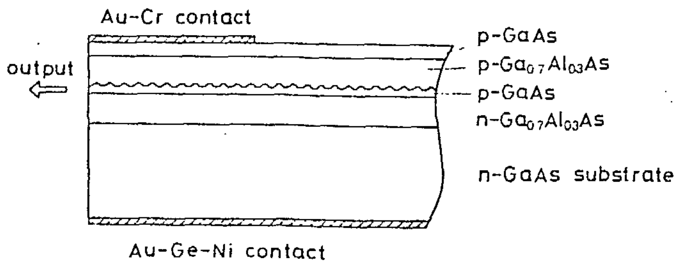

Figure 4.4 Schematic cross-section of the double-heterostructure distributed feedback laser

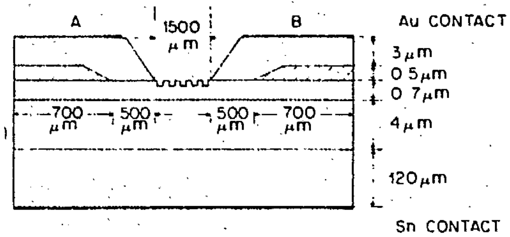

Figure 4.5 Schematic cross-section of the distributed Bragg reflector laser

Table 4.2 Parameters of LED's and Lasers to Be Used in WDM Systems

LED's

$\lambda(\mu m)$	$\Delta\lambda$ (nm)	$\frac{d\lambda}{dT}$ (nm/°K)	Peak power coupled into graded index fiber (mW)	Bandwidth (MHz)
0.8-0.9	35-60	0.3	0.2	50-200
1.0-1.3	75-100	0.3	0.2	50-200

LASERS

$\lambda(\mu m)$	$\Delta\lambda$ (nm)	$\frac{d\lambda}{dT}$ (nm/°K)	Peak power into coupled graded index fiber (mW)	Bandwidth (GHz)
0.8-0.9	2	0.3	5-10	2
1.0-1.3	2.5-3.5	0.3	5-10	2

DFB LASER

0.8-0.9	0.2	0.07	0.5-1.0	2

where n denotes the index of refraction of the waveguide. The majority of DFB lasers reported, operated in the form of third order gratings. This corresponds to a grating period of about 0.36 μm for an emission wavelength of 0.85 μm in the GaAlAs with an index of refraction of 3.5. The emission wavelength of DFB lasers can be tuned within the gain spectrum bandwidth of the alloy (typically ~ 20 nm) by adjusting the grating period. A change in grating period of 0.9 nm, for instance, will result in a shift of the peak emission wavelength by about 2 nm. The possibility of peak wavelength tuning as well as the feasibility of integration of DFB lasers on a single chip in fact were utilized effectively by Aiki et al[20] (see Figure 4.6). Six DFB lasers with different grating periods were integrated on a single chip and individual laser outputs were collected into a common launching waveguide. The lasing wavelengths were in the vicinity of 860 nm with wavelength separation of about 2 nm. The spectral width of the emission was 0.3 nm. The threshold current density of the lasers ranged from 3-6 kA/cm^2, the waveguide coupling efficiency was 30%, and the overall external quantum efficiency 0.3%. It is important to note that this integrated device will perform the function of a wavelength multiplexed source suitable for WDM applications.

2- Spectral width

The spectral width of LED's will depend on the type of dopant and dopant concentration in the active layer of the device. The spectral full width at half maximum (FWMM) of Si doped devices for instance is greater than those doped by Ge by about 30-40%. Higher dopant levels also result in increased amount of spectral broadening. The FWHM of LED's in the 0.8 - 0.9 μm range in general is within 35 - 60 nm. The spectral width of LED's increases to about 100 nm for devices in the vicinity of 1.3 μm. The ratio of the spectral width to peak emission wavelength however remains approximately the same indicating similar energy ranges of emitted photons.

In an ideal semiconductor laser, a homogeneously broad spontaneous spectrum and only a single excited Fabry-Perot spectral mode are expected. In practice, however, the wide gain spectrum, allows the cavity to support several modes separated by typically 0.1 - 0.3 nm which may lase with only slightly different gain. The overall spectral envelope of a laser operating under these conditions may be as wide as 2.0 - 3.0 nm.

Considerable effort has been devoted to achieve single mode operation. This was achieved successfully by improving the material uniformity of the device and by better waveguiding control of the emitted radiation. A channeled substrate laser[21]

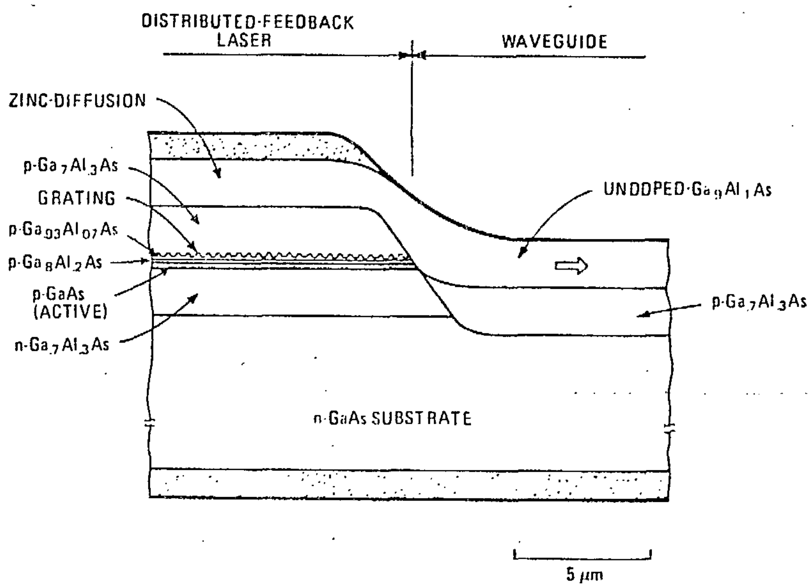

Figure 4.6 Cross-sectional view of waveguide coupled DFB lasers

is a typical representative of a device operating in a single mode with spectral width of about 0.3 nm. Single mode operation of standard Fabry-Perot lasers can also be obtained by using an external grating to provide an optical feedback mechanism for a given dominant mode. These devices are cumbersome, relatively inefficient and will not be further considered. Excellent mode control of the lasing emission is obtained by using DFB lasers. Good gain selectivity (very narrow spectral width, < 0.1 nm) in DFB lasers occurs because the threshold of an optical mode which differs from that supported by the Bragg reflection increases very rapidly. Calculations show that the expected spectral width of DFB lasers is approximately 0.1 nm. Nonlinear effects further reduce this value.

There are two reasons for requiring sources with narrow spectral width in WDM applications. Firstly, the number of optical sources which can be multiplexed into a given spectral range increases with a decrease in spectral width. It is anticipated that at least 10 sources can be multiplexed into a 20 nm wide gain spectrum bandwidth of GaAs using integrated DFB lasers. On the other side, the spectral bandwidth of LED's permits at most 3-5 sources to be multiplexed into the 0.8 - 0.9 μm or 1.0 - 1.3 μm regime. The determining factor, for multiplexing of several sources is the required crosstalk and the desired system signal-to-noise ratio. The second reason for requiring sources with narrow spectral width is that the material dispersion in fibers, at least in the 0.8 - 0.9 μm regime, can limit the maximum transmission rate capacity of the system. The effect is smaller in systems using longer wavelength sources.

3- Emission wavelength stability.

Another important parameter for consideration is the stability of peak emission wavelength with temperature, drive current and aging. Indeed, large shifts in peak emission wavelength can result not only in increased crosstalk, but can also lead to an increased insertion loss in several kinds of multiplexers. Narrow band interference filters for instance, can reject a a signal which under normal operating conditions would fall within the passband of the device. The above discussion thus points to a possible system requirement of efficient stabilization of the emission wavelength.

The emission spectrum of LED's and lasers changes with temperature owing to two distinct effects. Since the bandgap of the semiconductor decreases with increased temperature the spontaneous emission wavelength of a LED and the mean wavelength of the laser emission increases with temperature. Typical shifts in GaAs materials will yield a temperature coefficient of approximately 0.3 nm/°K. The second effect is due to the temperature dependence of the optical properties of the semiconductor. It can be shown that the wavelength of a spectral mode has a temperature coefficient

$$\frac{1}{\lambda} \cdot \frac{d\lambda}{dT} = \frac{1}{n} \frac{dn}{dT} \left(1 - \frac{\lambda}{n} \frac{dn}{dT}\right)^{-1}$$

with n denoting the index of refraction of the gain medium. For GaAs devices this gives a temperature coefficient of approximately 0.04 nm/°K.

The temperature coefficient of DFB lasers is between 0.03 - 0.07 nm/°K which indicates that the lasing is essentially determined by the grating period in the waveguide.

It should be noted that the threshold current in lasers also increases with temperature owing to reduction in the lasing gain mechanism. It appears that light sources, especially lasers, will require some form of temperature stabilization to ensure that the emission wavelength and the emitted power in lasers remain constant. Otherwise, the system should have sufficient tolerance for such changes. On the other side, the dependence of spectral emission on wavelength can be utilized effectively through the use of thermoelectric coolers to separate the emission wavelength of lasers which otherwise would not be in optimal spectral positions. A differential cooling of 30°C, for instance, will produce a wavelength shift of about 9 nm in Fabry-Perot lasers.

Heating in LED's also leads to broadening of the spectral width. The values of broadening depend on the type of dopant and dopant concentration, and it can be as large as 25%. Proper spectral positioning of various LED's in WDM systems for low crosstalk thus is important. The spectral emission of radiation will shift to longer wavelengths upon application of large drive currents. The effect is due to device heating and thus is equivalent to rise in the ambient temperature. A broadening in the spectral width of emitted radiation with high drive currents also has been observed.

The spectral properties of lasers under modulation conditions are also affected. Ikegami[22] reported that lasers show a very broad spectrum (3.0 - 4.0 nm) during the first few nanoseconds of an output pulse when modulated with a step increase in current. The above behaviour has been explained as due to the variations in the electron density during a period of an output pulse. The effect of pulsed modulation on lasing spectrum is of considerable significance since a broad spectrum might increase the crosstalk in system with closely spaced emission peaks. In addition the broad spectrum can limit the useful section length in a communication system as a result of material dispersion. The undesirable spectral broadening can be eliminated by maintaining the dc bias on the laser above the threshold at all times. The amount of bias above threshold is not critical and even a few mA is sufficient to give single mode operation.

A particular concern for reliable system operation is the effect of aging on emission wavelength and spectral width. Aging, in general, will result in a decrease in the radiative emission efficiency which in turn will require the drive current to be increased if the optical power output is to be preserved. Higher drive currents however will increase the device temperature and as a consequence the wavelength will shift to longer wavelengths. Device degradation in lasers can also lead in a loss of single mode operation resulting in a spectrum containing several Fabry-Perot modes.

b) <u>Other Properties</u>

1- Power Capabilities

High radiance GaAlAs LED's will couple about 200 μW of optical power into a graded index fiber (NA = 0.2) at current densities of about 5 kA/cm^2. Longer wavelength LED's are expected to achieve this performance.

The peak optical power coupled into fiber using GaAlAs laser as a light source is about 5 mW. This figure is expected to double in the near future.

The quantum efficiency of recently fabricated longer wavelength lasers is about 30-50% of GaAlAs lasers. Further improvements are anticipated.

The present power capability of DFB lasers is between 10-20% of Fabry-Perot lasers fabricated from the same material. Progress is expected.

2- Bandwidth

The bandwidth of LED's can be about 200 MHz with 0.5% efficiency. The efficiency however improves as the device bandwidth decreases. At 50MHz LED bandwidth the corresponding device efficiency is 5%.

The modulation frequency of lasers can be as high as 2 GHz with adequate dc prebias.

3- Linearity

The linearity of light sources is important for analog applications. For GaAlAs LED's total harmonic distortion figures of -30 to -33 dB were measured at 50% modulation depths.[28] The linearity of longer wavelength devices is expected to be the same. Laser linearity will improve with stable, single mode operation. Evidence to that effect already exists and distortion figures of less than -60 dB were measured at 5 mW output power.[29]

4- Reliability

At 0.8 - 0.9 μm, several laboratories have achieved LED and laser lifetimes in excess of 10,000 hrs. Extrapolated room temperature lifetimes of 10^6 hours for LED's and 10^5 hours for lasers are predicted from accelerated life tests at elevated temperatures. Further tests are required to assess the applicability of these lifetimes when lasers are operated at the output levels mentioned above in point 1. The reliability of longer wavelength light sources is improving rapidly and lasers with no degradation after 1,500 hours are already in existence. It is predicted theoretically that the reliability of longer wavelengths devices will be better than that of GaAlAs lasers. Although there is insufficient amount of information to assess the reliability of DFB lasers continuous efforts are being exerted to improve the overall performance of these devices.

4.4 PHOTODETECTORS

The choice of photodetectors for WDM system applications will depend on several parameters, such as: the wavelength regime for the operation, the transmission rate and the required signal-to-noise ratio. Two wavelength regimes (0.8-0.9 μm, 1.0-1.3 μm) and their coverage by photodetectors will be discussed. The 0.8-0.9 μm wavelength range is compatible with the presently available GaAlAs light source and Si detector technology. The 1.0-1.3 μm range has the advantage of reduced material dispersion in fibers leading to potentially higher transmission rate system in future.

4.4.1 <u>0.8 - 0.9 μm wavelength range</u>

Si detectors, both PIN and avalanche (APD) are used in the 0.8 - 0.9 μm region. The quantum efficiency of Si PIN photodiodes in this regime is about 85-95% for speeds ranging from dc up to 1 GHz.

The sensitivity of PIN photodiodes is usually restricted by the thermal noise of the preamplifier following the detectors and consequently these devices are preferred mainly in systems with low losses between the transmitter and the receiver. An improvement in performance desirable for long link (or high loss) applications is accomplished by exploiting the internal gain mechanism of avalanche photodiodes to raise the weak signal above the noise current of the preamplifier. Typically achievable gains in Si APD's are within 100 - 200 with breakdown voltages ranging from 100-300V.

An important parameter in determinimg the quality of APD is the noise current spectral density given by:

$$i_n^2 = 2e\,(I_{ph} + I_d)\,M^2F + 2eI_s$$

where I_{ph} and I_d denote the bulk photo and dark currents before multiplication respectively and M gives the avalanche gain. I_s denotes the surface leakage current. The excess noise factor F is equal to

$$F = kM + (1 - k)\left(2 - \frac{1}{M}\right)$$

$$2 + kM \text{ for } M >> 1,\ k << 1$$

with k denoting the effective ratio of the ionization rates for electrons and holes. For good Si APD's $k \approx 0.02 - 0.04$. The bulk dark current in APD's is within 0.1-0.5nA. The surface current leakage does not undergo multiplication and is within 10-50 nA.

The risetime of APD's can be as low as 0.1ns with quantum efficiencies ranging from 30-95% depending on the device type. Diffused guard ring and reach-through type APD's are the most widely available structures.

4.4.2 1.0-1.3 μm wavelength range

The quantum efficiency of standard top illuminated Si photodiodes for wavelengths above 0.9μm drops rapidly and at 1.06μm, it is only about 10-20%. By designing devices with side entry illumination, however, the quantum efficiency can be improved to a figure of about 50% at 1.06 μm. Such photodiodes can be effective at most up to 1.1 m beyond which the absorption coefficient of Si is very small.

Detectors made of Ge and of alloys of III-V compounds can be used for the longer 1.0-1.3μm regime. Ge photodiodes are effective between 0.6-1.6μm with peak efficiency about 50% near 1.5 m. The risetime of Ge APD's can be as low as 0.12ns, the gain as high as 200 with breakdown voltages of about 40V.

Due to the narrow energy gap in Ge, however, the dark current in Ge photodiodes is considerably higher than that in Si. Bulk dark currents of about 100nA in Ge detectors, as opposed to 0.01 nA in typical Si devices, are common. The effective ratio of ionization rates k is also higher than that in Si, typically $k \approx 0.5$. As a result the excess noise generated by the multiplied dark current in Ge APD's can be very high. Studies, indicate that at low and moderate transmission rates the non avalanching Ge PIN photodiode is preferable to the APD because of the latter's enhanced shot noise. Reduced dark currents and thus higher sensitivities can be obtained both in Ge and Si photodetectors by cooling.

Although photodetectors fabricated from alloys of III-V compounds are not commercially available now there is evidence that this type of devices will be suitable for longer wavelenth applications. Photodiode structures of InGaAs[23] and GaAsSb[24] have already been fabricated on GaAs substrates. These devices are optimized for operation in Nd:YAG laser systems at 1.06μm. Quantum efficiencies of 50%, response times of 0.25ns or less have been measured both for GaAsSb junction photodiode and InGaAs Schottky barrier photodiodes. Both types of devices have been operated as avalanche devices.

A successful fabrication of APD's from quarternary GaInAsP alloy has been reported recently by Hurwitz and Hsieh[9] and by Pearsall et al.[10] Gains of 12, risetimes of less than 0.15ns, and quantum efficiency in excess of 40% have been measured at 1.15 m. It is important to notice that the dark current of the GaInAsP (0.02nA) fabricated by Pearsall et al. was almost three orders of magnitude less than that of Ge APD and only slightly higher than that of best Si devices. The breakdown voltage of the GaInAsP was 22V and a gain of 100 was measured. The quantum efficiency between 1.0-1.3μm was 70-75%. The quarternary is ideally suited for the 1.0-1.3μm regime since the alloy bandgap can be varied continuously from 0.92μm to 1.6μm with good lattice matching to InP substrate. Non-avalanching photodiodes of this material have been already fabricated.

4.4.3 Other interesting devices and structures

Photodetectors based on electroabsorption (Franz-Keldysh) effects have also been reported. These devices will be useful in integrated optical circuits for signal processing and fiber optics communications. In principle, devices based on electroabsorption effects can be integrated in a compact wavelength demultiplexer.

A multisection photodector operating in the 0.8-0.9μm regime was proposed by J.C. Dyment et al.[25] Each section of the photodetector is expected to respond only to selectively absorbed optical wavelengths. To avoid crosstalk due to spectral overlap in the detectors a threshold amplifier responding above a preset signal amplitude at a given wavelength would have to be incorporated in the demultiplexer. Multiplexing rates in excess of 1 Gbits/s are expected.

A GaAs waveguide detector compatible with 1.0-1.1μm range and operating on electroaborption principles has been reported by Nichols et al.[26] The internal quantum efficiency of the device was 23% at 1.06μm. Progress in monolithic APD fabrication has also been reported.[27] Such devices are expected to find practical use in WDM systems. Takahashi et al reported a monolithic 1x10 APD array of Si APD's with voltage breakdown at 131 V and APD gains in excess of 50. The variations in breakdown voltage and gain were less than $\pm 0.3\%$ and $\pm$ 2% (at gain 56) respectively. The primary bulk dark current was approximately 0.05 nA.

4.5 SUMMARY

In this section the review of the present state-of-art of optoelectric components has been made with an emphasis on WDM system applications. Considerable attention has been paid to expected developments in the longer wavelength (1.0-1.3 μm) regime. The rationale for longer wavelengths operation is twofold. Firstly, WDM operation at longer wavelengths allows the available spectral range to increase from that provided by the 0.8-0.9 μm regime. Secondly, decreased attenuation and material dispersion in the 1.0-1.3 μm regime allows transmission rates and distances to increase significantly from those attainable in the 0.8-0.9 μm regime.

As far as the transmission medium is concerned, future WDM systems will use predominantly multimode graded index fibers. The fabrication technology of this type of fiber is well developed and the fiber handling (splicing, connectorization, source to fiber and source to detector coupling) is relatively easy.

The choice of light sources for WDM system applications will depend on several design parameters such as the emission wavelength range, the number of channels transmitted, the spectral stability, the crosstalk and the signal-to-noise ratio.

The peak emission wavelength of light sources will be determined primarily by the alloy composition of the active layer. The use of alloys of III-V compounds assures the necessary coverage of the two low loss regimes in the fiber (0.8-0.9 μm, 1.0-1.3 μm). Devices in the 0.8-0.9 μm regime will be fabricated from GaAlAs while those in the 1.0-1.3 μm wavelength range will have the option of using several alloys of III-V binary compounds. Secondary shifts in the peak emission wavelength will occur due to doping of the active layer. Owing to variations both in the alloy composition and in dopant incorporation the emission peak of LED's and lasers will differ from device to device by about 2-3 nm. Practical system designs should make allowance for such wavelength variations, in particular, in the view of device replacement in case of failure. The wavelength of lasing emission in DFB lasers fabricated from a given material can be controlled to a high degree of reproducibility. This is because the optical feedback in DFB lasers is determined by the grating period which can be prepared in a controllable manner. On the other extreme, it is anticipated that integrated DFB lasers will permit as many as 10 channels to be multiplexed into a 20 nm wavelength interval. In principle, staggered multiplexing of several integrated DFB laser chip could lead to systems with 20-30 channels. The performance of such systems will be limited by the interval multiplexing efficiency between the separately integrated elements. The efficiency of a single integrated element with 6 sources presently is 0.3%. With better coupling efficiency this figure will probably increase to 5%. With estimated 5 dB loss between the discrete elements the overall efficiency of staggered systems will be 1%.

The spectral width of Fabry-Perot lasers is between 0.3 - 0.7 nm for a single mode and 2.0 - 3.5 nm for multimode operating devices. With conservative 10 nm channel spacing 10 channels can be multiplexed into 100 nm wide spectral band. The low loss and the low material dispersion regime between 1.0 - 1.3μm in fibers therefore could accept as many as 30 channels. The efficiency of the multiplexer and crosstalk requirements may again limit the overall system performance.

The wavelength separation of different channels in practical systems in addition to the spectral width, will also be determined by the dependence of the emission peak on the operating temperature range, drive currents and ageing. The emission peak of Fabry-Perot lasers and LED's will shift to longer wavelengths with increasing temperature at rate 0.3 nm/°K. A change of 20°C in the ambient temperature for instance will result in a wavelength shift of as much as 6 nm. If wavelength shifts of this order cannot be tolerated, temperature stabilization will be required. Most of the lasers will also be stabilized against threshold current variations and care will have to be taken to ensure that these two distinct requirements will not be in conflict. The requirement for temperature stabilization in LED's will probably not be as severe as in lasers provided increased spectral broadening with temperature can be tolerated. Integrated DFB lasers ($d\lambda/dT$ = 0.05 nm/°K) in systems with extremely narrow wavelength separation will also require temperature stabilization. It should be noted that the temperature dependence of the emission peak can be utilized to increase the wavelength separation between different lasers in a given system. Differential cooling by thermoelectric coolers will bring the desired result.

Modulation currents in lasers biased below threshold will increase the spectral width. Aging can result in similar phenomena with changes on the order of 2 nm in Fabry-Perot devices. There is an insufficient amount of information on similar effects in DFB lasers although some tolerance against possibly similar changes would have to be included in the system design.

As per discussion given above, the minimum separation of roughly 10 nm between wavelengths of different Fabry-Perot devices can now be justified. Allow 2 nm for temperature changes ($\sim \pm$ 3°C), 2 nm for variation from device to device in case of replacement, 2 nm for increase in spectral width due to aging and modulation and 2 nm for spectral width. The total margin in crosstalk is therefore only 2 nm. Similar considerations can be made for other DFB lasers and LED's. On the basis of power capability lasers are preferred to LED'S. Lasers will couple 5 mW of power into fibers while typical LED's about 200 μW. The efficiency of DFB lasers is about 10-20% that of Fabry-Perot structures and other considerations such as the available wavelength regime, spectral width, stability and reliability will dictate the choice between the two light sources.

In reference to detectors, Si-PIN's and APD's will be used in the 0.8-0.9μm regime. The choice between the two detectors will depend on the transmission rate and the required system sensitivity. For shot noise limited system PIN photodiodes are adequate. For systems limited by the preamplifier noise APD's will be preferred. In the 1.0 - 1.1 μm regime specially developed side entry Si detectors can be used. These devices will compete with detectors fabricated from Ge or from alloys of III-V compounds. As far as the excess noise is concerned Si detectors have the advantage.

For immediate applications beyond 1.1 μm Ge detectors are commercially available. APD's made of Ge however suffer from high excess noise and calculations indicate that the use of a non-avalanching detector, might be preferable.

Avalanche photodiodes fabricated from alloys of III-V compounds are particularly promising in the 1.0-1.3 μm regime. The quaternary alloys permit the response of ther APD to be tailored for a specific wavelength range. Dark currents comparable to that of Si APD's and 3 orders of magnitude lower than that of Ge APD's in III-V alloys have recently been achieved. Further improvements in III-V photodetector technology are expected.

Integrated photodetectors based on electroabsorption effects have potential applications in wavelength demultiplexing of optical signals. Their practical implementation however remains to be demonstrated.

4.6 REFERENCES

4.1 J.P. Conradi, F.P. Kapron and J.C. Dyment, IEEE Trans. Elect. Dev. ED-25, 180 (1978)

4.2 T. Kimura and K. Daikoku, Opt. Quant. Elect., 9, 33 (1977).

4.3 M. Horiguchi and H. Osanai, Electron Lett 12, 310 (1976)

4.4 F.P. Kapron and D.B. Keck, Appl. Opt. 10, 1519 (1971)

4.5 L.G. Cohen and S.D. Personick, Appl. Opt. 14m 1357 (1975).

4.6 W.G. French, Appl. Opt. 15. 1803 (1976).

4.7 J.P. Wittke, M. Ettenberg and H. Kressel, RCA Review 37, 159, (1976).

4.8 C.T. Nuese, J. Elect. Mat. 6, 253 (1977).

4.9 C.E. Hurwitz and J.J. Hsieh, Tech. Dig. Topical Meeting on Integrated and Guided Wave Optics, Jan. 1978, Salt Lake City, Utah, MC-1.

4.10 T.P. Pearsall, E. Duda, M. Papuchon and R. Goulet, Techn Dig. Topical Meeting on Integrated and Guided Wave Optics, Jan. 1978 Salt Lake City, Utah, MC-2

4.11 T.P. Pearsall, B.I. Miller, R.J. Capik and K.J. Bachman, Appl. Phys. Lett 28, 499 (1976)

4.12 A.G. Dentai, T.P. Lee, C.A. Burrus and E. Buehler, Electron. Lett 13, 484 (1977).

4.13 C.C. Shen, J.J. Hsieh and T.A. Lind, Appl. Phys. Lett. 30, 353 (1977)

4.14 R.E. Nahory, M.A. Pollack, E.D. Beebe, J.C. DeWinter and R.W. Nixon, Appl. Phys. Lett 28, 19 (1976).

4.15 T. Yamamoto, V. Sakai, S. Akiba and Y. Suematsu, Electron Lett. 13, 484 (1977).

4.16 C.A. Burrus and B.I. Miller, Opt. Commun., 4, 307 (1971).

4.17 F.D. King, A.J. Springthorpe, and O.I. Szentesi, Tech. Dig. Int. Electron Device Meeting, Washington, D.C., December 1975, p. 4.480.

4.18 M. Nakamura, K. Aiki, T. Umeda, Y. Yariv, H.W. Yen and T. Morikawa, Appl. Phys. Lett, 25, 487 (1974)

4.19 F.K. Reinhard, R.A. Logan and C.V. Shank, Appl. Phys. Lett, 27 45 (1976)

4.20 K. Aiki, M. Nakamura, and J. Umeda, Appl. Phys. Lett, 29, 506 (1976).

4.21 K. Aiki, M. Nakamura, T. Kuroda and J. Umeda, Appl. Phys. Lett 30, 649 (1977).

4.22 T. Ikegami, IEEE Conference on Optical Fibre Communications, London 1975.

4.23 G.E. Stillman, C.M. Wolfe, A.G. Foyt, and W.T. Lindley, Appl. Phys. Lett., 24, 8 (1977).

4.24 M.C. Boissy, D. Diguet, J. Hallais and C. Schemaei, Int. Phys. Conf. Ser. No. 33a, 427 (1977).

4.25 J.C. Dyment, F.P. Kapron and A.J. Springthorpe, Inst. Phys. Conf. Ser. No. 24, 200 (1975).

4.26 K.H. Nichols, W.S.C. Chang and C.M. Wolfe and G.E. Stillman, Appl. Phys. Lett 31, 631 (1977)

4.27 U. Takahahsi, S. Takamiya and S. Mitsui, 100C, 1977, Tokyo, Japan, A3-2.

4.28 F.D. King, J. Straus, O.I. Szentesi and A.J. Springthorpe, Proc. IEE 123, 619 (1976).

4.29 R. Ito, Tech. Dig., CLEOS, February 1978, WAA1.

References not cited

Fibers:

1. S.E. Miller, E.A.J. Marcatili and T. Li, Proc. IEEE 61, 1703 (1973).
2. J.A. Arnaud, "Beam and Fiber Optics", Academic Press 1976.
3. W.B. Allan, "Fiber Optics", Plenum Press, 1973
4. K. Barnoski, Ed, "Fundamentals of Optical Fiber Communications", Academic Press, 1976.
5. D. Gloge, Ed, "Optical Fiber Technology", IEEE Press 1976.

Sources:

1. H. Kressel and K. Butler, "Semiconductor lasers and heterojunction LED's, Academic Press 1977.

2. H. Kressel, "Electroluminescent Sources for Fiber Systems", in Fundamentals of Optical Fiber Communications" ed M. Barnoski, Academic Press, 1976.

3. C.H. Gooch, "Injection Electroluminescent Devices, John Wiley and Sons, 1973.

4. M.P. Panish, Proc IEE 64, 1512 (1976).

Detectors:

1. H. Melchior, J. of Lumm. 7, 390 (1973).

2. A.D. Lucas, Proc. IEE, 123, 623 (1976).

3. H. Melchior, M.B. Fisher, F.R. Arams, Proc IEEE, 58, 1466 (1970).

5. MULTIPLEXING AND DEMULTIPLEXING DEVICES

5.1 INTRODUCTION

A schematic diagram of a simple WDM multiplex system is shown in Figure 5.1. Beam splitters at the input end combine the optical signals from m different sources for transmission while at the output they split the received signal into m separate output beams. A suitable bandpass filter in front of each detector selects the desired wavelength. If the detector in the receiver circuitry is sufficiently narrowband the need for filters in the receiver is eliminated. Unfortunately, the response of photodetectors is broadband and wavelength discrimination is required. With the arrangement shown in Figure 5.1 the minimum insertion loss per channel is of the order of m^{-2} which except for the m=2 case would represent an unacceptably large insertion loss.

To achieve lower insertion losses techniques specially tailored for efficient wavelength division multiplexing have to be considered. The results of such considerations are presented in this section.

This section is divided into five sub-sections. Following the introduction some general considerations on mux/demux design are given in section 5.2. The feasibility of several multiplexing schemes and techniques is discussed in section 5.3. The performance of some recently fabricated multiplexing devices is described in section 5.4 The results of these considerations are summarized in section 5.5

5.2 GENERAL CONSIDERATIONS

The basic design problem in a multiplexer is to provide a low loss path from each source to the output fiber. Ideally, the sources should be monochromatic, with zero spectral overlap. In practical systems however, a certain degree of spectral overlap can always be tolerated.

The requirements on demultiplexers are more demanding. In addition to providing a low loss optical path between the input and output signals the demultiplexers must also separate efficiently signals of different wavelength. To avoid crosstalk, the amount of undesired signal at each output port must also be minimized.

The two devices in most cases however are interchangeable i.e. they are reciprocal. Their use in either configuration will depend on the maximum allowable insertion loss, crosstalk, and the practicability of a given arrangement geometry.

5.3 MULTIPLEXING AND DEMULTIPLEXING TECHNIQUES

The list of devices which can be used for efficient multiplexing of optical signals is given below. The list is by no means exhaustive as it represents instead a cross section of possible and presently available methods by which low loss optical multiplexing can be achieved. The development of multiplexers based on different techniques and technology is expected. Multiplexing is currently achieved by using:

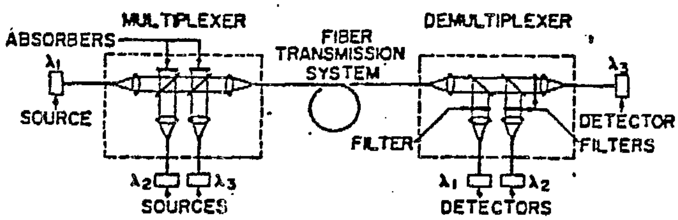

Figure 5.1 Schematic diagram of a multiplexed transmission system using beam splitters

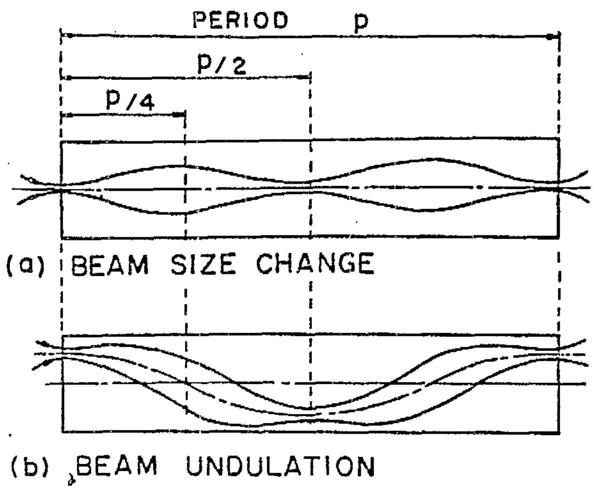

Figure 5.2 Beam transformation by a rod lens

- light focusing rods (GRIN rods)[1,2]
- multifiber combiners[3]
- angularly dispersive elements (prisms, gratings)[4,5]
- devices based on wavelength dependent reflectivity and transmission (interference filters, multiple gratings)[4]

The devices listed above will each multiplex into a common output port a number of separate optical sources which will be attached at the input end of the multiplexer. A different approach to the problem of low loss multiplexing is achieved by fabricating a number of optical sources each with different emission wavelength on a common substrate with outputs integrated into a common waveguide. The fabrication and the performance of such a device has been given earlier in section 4. Although integrated optical devices offer promise for efficient optical multiplexing their development is at early stages and further work is required to establish their availability in large scale applications.

For demultiplexing the devices considered are based on:
- wavelength dependent angular deviation (prism, gratings)[4;5]
- interference effect, i.e. wavelength dependent reflectivity and transmission (phase gratings)[4]

The discussion on these two topics, both for multiplexing and demultiplexing devices is based on a recent publication by Tomlinson[4].

5.3.1 Multiplexers

GRIN rods

The use of radially graded refractive index rods[1] (GRIN rods) for multiplexing applications has been described by Kobayashi et al.[2]

The major function of rod lenses in transforming the light beam is to achieve a periodic change in beam diameter and/or to achieve a periodic beam position change or beam undulation. (See Figure 5.2) By combining these changes with reflective or refractive elements positioned at the end facets of GRIN rod lenses, efficient branching, coupling multiplexing, and demultiplexing devices can be fabricated.

A multiplexer designed to multiplex up to four input beams using GRIN rod lenses was described recently by Sugimoto et al.[6] (See Figure 5.3) The insertion loss of the multiplexer was about 3 dB.

Multifiber combiners

The fabrication and the performance of an efficient power combiner for optical fiber systems was described by K. Hill et al.[3] The optical combiner could multiplex three sources to a single trunk with insertion loss between any of the three fibers and the trunk of approximately 1 dB. The device can accomodate several additional sources without incurring excessive additional loss. The optical isolation between ports is greater than -50dB. (See Figure 5.4).

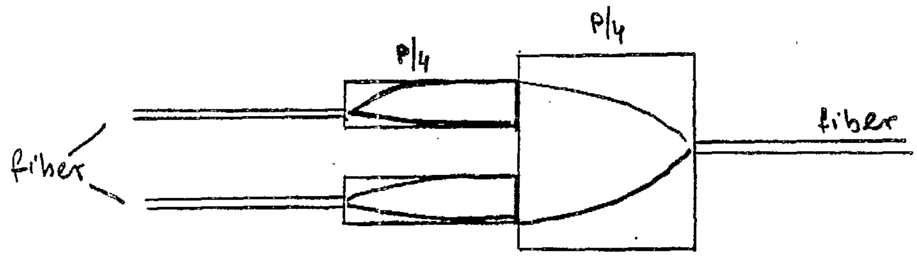

Figure 5.3 GRIN rod multiplexer (side view)

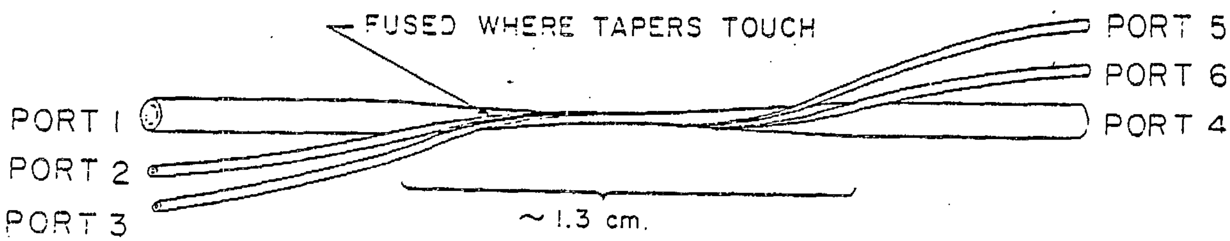

Figure 5.4 Optical multifiber combiner

Unequal feeder to trunk and trunk to feeder characteristics are achieved by introduction of geometrical asymmetry in the coupling process by the use of fibers with different diameters. The principle of operation is as follows:

Most of the light launched as guided modes in one of the fiber smaller arms radiates out of its core into the narrowing taper is where ittransformed into cladding modes. The light propagates to the f region oexpanding tapers which transform the light back into guided hich modes, win turn propagate in the cores of the different fibers. The on proportiof the total launched light that emerges in each output arm is ed determinapproximately by the different cross sectional areas that the comprisetaper region of the device. Since the trunk fiber has the cross largest section it will accumulate the major portion of the light.

Devices based on refractive and interference effects

The use and the performance of these devices in WDM will be discussed in connection with the design of demultiplexers.

5.3.2 Demultiplexers

The discussion on angularly dispersive devices as well as on devices based on interference effects is based on the following assumptions:

- All inputs and outputs are on fibers of identical characteristics. As shown in Reference 4 however advantages in certain cases can be gained by attaching sources (or detectors) directly to the multiplexer (or demultiplexer). On the other hand having all inputs/outputs on fibers has the advantage that the multiplexer/demultiplexer is a self standing passive device which does not need to be replaced in case of a source/detector failure. The optimal arrangement will depend on particular circumstances of system design.

- It is further assumed that the system has unity magnification except when mentioned otherwise. This assumption allows to use identical input/output optics, a considerable manufacturing simplicity.

To avoid duplication of terminology the term multiplexer will be used freely for both multiplexers and demultiplexers except where the two devices have to be specifically distinguished.

Angularly Dispersive Devices

Angularly dispersive elements can be represented as shown in Figure 5.5. The signal from the input fiber is collimated, passed through the dispersive element and the resulting beams are then focused on the output fibers (possibly output detectors). The linear dispersion at the position of the output fibers is

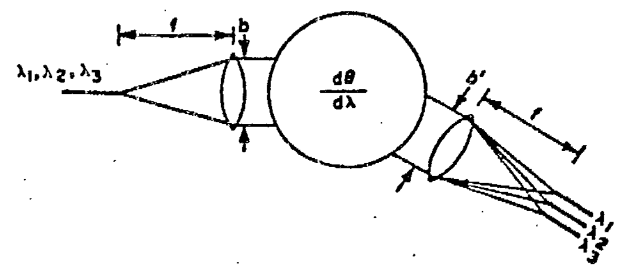

Figure 5.5 Schematic drawing of a multiplexer using an angularly dispersive element

$$\frac{dx}{d\lambda} = f. \frac{d\theta}{d\lambda} \tag{5.1}$$

with f being the focal length of the focusing optics, and $\frac{d\theta}{d\lambda}$ being the angular dispersion of the dispersive element.
For

$$\frac{dx}{d\lambda} \Delta\lambda \geq d \tag{5.2}$$

where $\Delta\lambda$ denotes the wavelength separation between different sources and d gives the diameter of the output fiber, the separation between the demultiplexed output beams is greater than the output fiber diameter and consequently the crosstalk and the insertion loss is equal to zero. In practice, it is more realistic to require that the output signals be separated by the diameter of the fiber claddings rather than that of the core. In any case equation 5.2 can be considered to give a lower limit on the required dispersion which correspondingly will determine the lower limit on the required dimensions of the multiplexer.

To capture all light from the input fiber the minimum collimator diameter b is given from equations 5.1 and 5.2 by

$$b \geq \frac{2D}{\lambda(d\theta/d\lambda)n'} \quad \text{with } D = \frac{\lambda(NA)d}{\Delta\lambda} \tag{5.3}$$

with NA denoting the numerical aperture of the fiber and n being the refractive index of the medium between the dispersive device and the collimating and the focusing optics. In addition, to avoid overfilling the aperture of the output fiber, it is important to keep the spread of the output beam to a fraction of the collimator diameter. The fractional increase in the beam diameter is approximately

$$S \sim (1 + m) \frac{Wd\ (NA)}{b^2\ n'} \tag{5.4}$$

with W being the total path length from the output of the collimator to the input of the focusing optics. For efficient operation it is required that S << 1. In the following section the performance of some selected angular dispersive elements is reviewed.

Prisms

Schematic diagrams of prism multiplexers are shown for two configurations in Figure 5.6. The angular dispersion of a prism is given by:

$$\frac{d\theta}{d\lambda} = \frac{d\theta}{dn} \cdot \frac{dn}{d\lambda} \qquad (5.5)$$

In equation 5.5 the first factor on the right depends on the geometry of the arrangement, while the second factor characterizes the dispersive power of the material from which the prism is made. In the position of minimum deviation angle[7]

$$\frac{d\theta}{d\lambda} = \frac{B}{n'b} \cdot \frac{dn}{d\lambda} \qquad (5.6)$$

where B is the length of the base of the prism. The minimum size of the prism is equal to

$$B = \frac{2D}{\lambda \frac{dn}{d\lambda}} \qquad (5.7)$$

independent of the refractive index of the immersion medium.

According to Hata, large dispersion and low absorption loss, preferable for the prism material, is achieved by using a semiconductor which has a fundamental absorption edge at a point just outside the wavelength under consideration.[5] CdS and $Ga_{0.8}AL_{0.2}As$ are suggested for the 0.77 - 0.87 μm band, while SiO_2, CdS, CdSe and $Ga_{0.9}Al_{0.1}As$ are to be used for multiplexing between 0.85 μm and 1.05μm. Other II-VI semiconductors, Se and chalconigenide glasses[4] (As_2S_3) can also be used.

Table 5.1 shows[5] the estimate of the effective size of a multiplexer with a CdS or $Ga_{0.8}Al_{0.2}As$ prism calculated with 1.2 dB detector loss and 30 dB allowable crosstalk. Table 5.2 gives[5] the effective size of demultiplexers with SiO_2, CdSe, $Ga_{0.9}Al_{0.1}As$ prisms in the 0.85 μm and 1.05 μm band for the same crosstalk and detector loss. An increase of at most 15% in the size of the prism and of the focusing optics is expected with an increase of the source halfwidth from 2nm to 30nm. Consequently, the dimensions of the multiplexer are relatively insensitive to broad spectral changes which suggests a possible use of LED's in the 0.85 μm to 1.05 μm range.

Blazed Gratings

The angular properties of a grating are described by the following grating equation.

a.

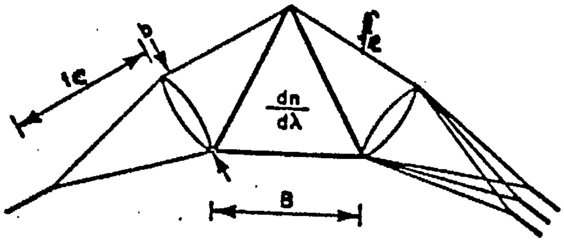

b.

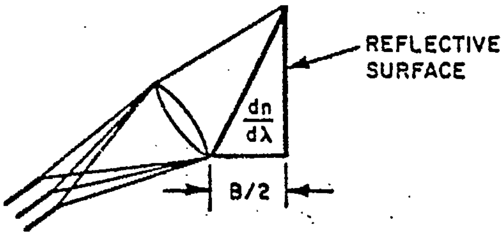

Figure 5.6 Multiplexers using prisms

TABLE 5.1 Multiplexer effective sizes*

Prism materials	$\Delta\lambda$ (nm)	CHANNEL SEPARATION 10	20	30	40	60
CdS	2	38.62	22.53	13.87	9.57	5.34
	12	•	•	15.42	10.0	5.44
$Ga_{0.8}Al_{0.2}As$	2	16.35	7.32	6.34	2.70	1.21
	12	•	•	7.84	2.78	1.28

* Effective sizes l_t of a CdS or $Ga_{0.8}Al_{0.2}$ As prism in 0.8 μm band d = 0.1 mm, N.A. of fibre = 0.145, separation length among detectors 1 mm and wavelength at minimum deviation angle 770 nm (in mm x 10).

TABLE 5.2 Demultiplexer effective sizes*

Prism materials	$dn/d\lambda$ at 0.85μm $10^{4}(cm^{-1})$	f_c (mm)	B (mm)	f_f (mm)	l_t (mm)
SiO_2	0.016	21.0	18.6	111.0	150.6
CdS	0.211	3.7	2.0	20.1	25.8
CdSe	0.55	1.1	0.5	6.1	7.7
$Ga_{0.9}Al_{0.1}As$	1.19	1.2	0.4	6.9	8.5

*Incident angle = 65.6 for multiplexing between 0.85μm and 1.05μm. The angle of minimum deviation is 860 nm and $\Delta\lambda$ = 2 nm

f_c - focal length of the collimating lens
f_f - focal length of the focusing lens
B - base of the prism
$l_t = f_c + f_f + B$.

$$\sin i + \sin \quad = \frac{k\lambda}{n'\Lambda} \tag{5.8}$$

where Λ is the grating period, k is the order of diffraction and i and θ are the angles of the incident and of the refracted beams respectively measured from the normal to the grating surface. A grating is said to be in the Littrow configuration (autocollimation) when $i = \theta$ (Figure 5.7). This mounting also minimizes astigmatism and utilizes the same input and output optics. The angular dispersion of the grating for a constant angle of incidence is equal to:

$$\frac{d\theta}{d\lambda} = \frac{\sin i + \sin\theta}{\lambda \cos \theta} \tag{5.9}$$

which for the Littrow configuration becomes

$$\frac{d\theta}{d\lambda} = \frac{2}{\lambda} \tan \theta \tag{5.10}$$

In general, all diffracted orders contain a part of the incident energy, with the 0th order (which does not diffract at all) containing the most of it. The efficiency of the grating however, can be increased by tilting the reflecting elements with respect to the grating surface. In this case a high power concentration can be obtained in any one of the orders.

Specifically, a triangular profile grating (echelette) concentrates all the energy in the 1st order. The wavelength for which all other diffraction orders are extinguished is called the blazed wavelength (λ BL) and the angle ϕ_{BL} the angle of the tilt, is called the blaze angle.[8,9]

The efficiency of the grating at its blaze angle is usually insensitive to the polarization of the input light.[4]

The minimum collimator diameter for the Littrow mount is given from equations 5.3 and 5.10 by

$$b = \frac{D}{n' \tan \theta}$$

As equation 5.11 shows the collimator size decreases with the use of immersed optics.

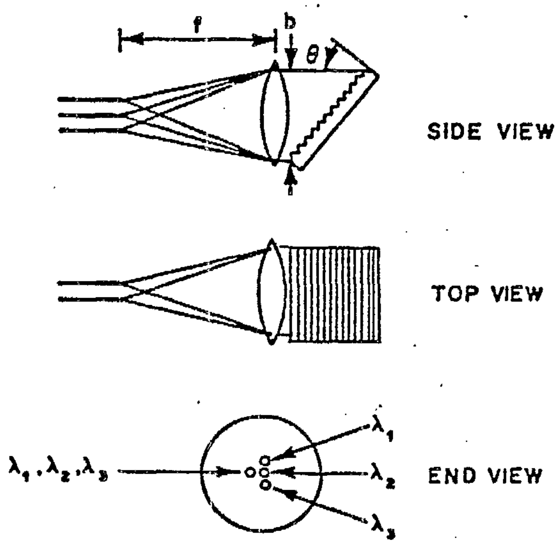

Figure 5.7 Multiplexer using a blazed plane reflection grating

The fractional beam spreading S is equal to:

$$S = 2\,(1 + m)\,\tan^2\theta \quad \frac{(\Delta\lambda)}{\lambda} \tag{5.12}$$

Equations 5.11 and 5.12 determine the new restriction on the size of the collimator

$$b \geq \frac{D}{n'} \left[\frac{2(1 + m)}{S\,\lambda} \quad \Delta\lambda \right]^{1/2} \tag{5.13}$$

The maximum wavelength range (m-1) $\Delta\lambda$ that can be covered without overlapping of orders is

$$(k+1)\,\lambda = k\,(\lambda + (m-1)\Delta\lambda) \tag{5.14}$$

or $\lambda = (m-1)\Delta\lambda$ in the first (k=1) order.

Blazed reflection gratings with at least 75% reflection efficiency (1.2 dB insertion loss) into a given order are manufactured.[10] To achieve the groove shape required for high efficiency at each specific wavelength application an original would probably have to be made on a ruling machine. Following this operation, however, cast high quality replicas could be made and mass produced. Practical systems would have to take into account the influence of grating imperfections, of spurious ghosts and of stray light which may reduce the overall signal-to-noise ratio and crosstalk.

Thick Phase Gratings

Diffraction grating will also result from a periodic variation of the index of refraction in a material.[11] A thick phase grating is characterized by an index modulation of the form.

$$n\,(x,y,z) = n' + n_0 \cos\left(\frac{2\pi}{\Lambda}\,(x \sin\theta + 2 \cos\phi)\right) \tag{5.15}$$

The dashed lines in Figure 5.8 are the planes of constant refractive index. More complicated devices with multiple periodicities can also be considered. Such devices are referred to as multiple gratings or holograms.

The equation of a grating with index variation of the form of equation 5.15 is given by

$$\sin i - \sin\theta = \frac{\lambda}{n'\Lambda} \quad \sin\phi \tag{5.16}$$

For a fixed wavelength

$$\frac{d\theta}{di} = \frac{\cos i}{\cos \theta} \tag{5.17}$$

so that to minimize distortion in the image $\theta \approx \pm i$ is required as in the case of the blazed grating.

Under the Bragg condition

$$\cos (\phi - i) = \frac{\lambda}{2n'\Lambda} \sin \phi \tag{5.18}$$

which is the maximum efficiency condition in thick gratings, the incident and the scattered waves propagate at equal angles with respect to grating planes, corresponding to specular reflection. To satisfy both, the requirement on the minimal distortion and on the Bragg condition ϕ must be equal to $\phi \simeq 0$ or $\pi /2$. A grating under the $\phi = 0$ case (grating planes parallel to the faces) is referred to as a reflection filter, while that for $\phi = \pi /2$ (grating planes perpendicular to the faces) is known as a transmission filter. (See Figure 5.9).

From the formula for the angular dispersion

$$\frac{d\theta}{d\lambda} = \frac{-2 \tan\theta}{\lambda} \cdot \sin \phi \tag{5.19}$$

it is noted that for $\phi = 0$, the reflection filter case, there is no angular dispersion at all, and the wavelength selectivity of the grating results from the wavelength dependence of reflectivity and transmission. For $\phi = \pi/2$ the formula for angular dispersion is the same as that for blazed grating and thus the wavelength selectivity is the result of a combination of angular dispersion and wavelength dependent reflection and transmission.

To avoid significant beam spreading the gratings are used at $\phi = \pi/4$ inclination to the input beam. At this angle the required collimator size in terms of a specified beam spread is given by

$$b = \frac{D}{n'} \left[\frac{2(m-1)\Delta\lambda}{S\ \lambda} \right] \tag{5.20}$$

In general, the collimator size for the grating will be determined by the beam spreading problem.

As discussed by Kogelnik the characteristics of thick gratings at $\phi = \pi/4$ are dependent on the polarization of the input light.[12] Such polarization dependence constitutes a big disadvantage for the use of thick gratings since a fixed linear polarization of optical signals in present fiber optics systems cannot be assured.

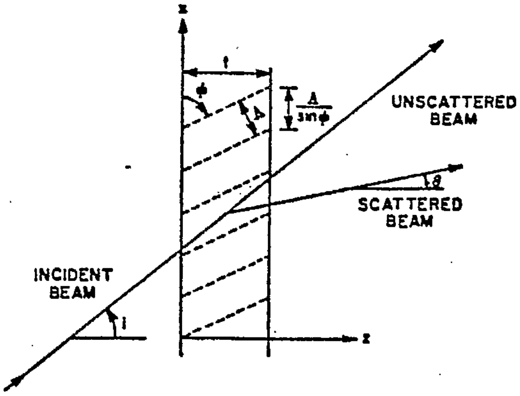

Figure 5.8 Cross-section of a thick phase grating

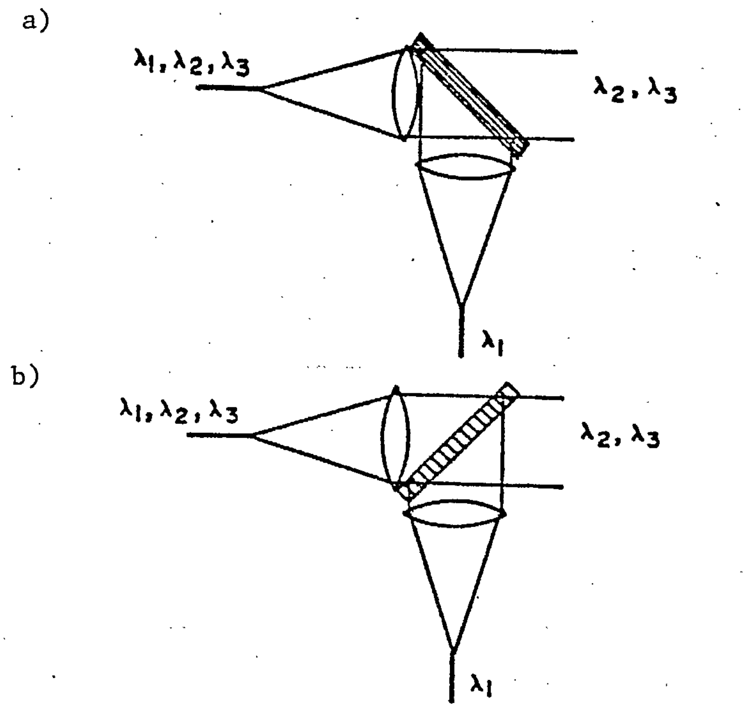

Figure 5.9 Multiplexers using simple thick grating
a) reflection filter
b) transmission filter

It should further be noted that a simple thick grating selects only one wavelength and a m-channel multiplexer would require at least m-1 separate gratings and collimators. Apart from increased system complexity it can be expected that accumulated insertion losses of the gratings will limit the number of transmitted signal channels. The preparation of a suitable reflection filter by multilayer coating techniques also represents a major difficulty. As discussed by Tomlinson[4] to achieve low insertion loss in the transmit and reject channels, many layers with small refractive index differences have to be deposited with great precision. Under such extreme requirements the filter is highly susceptible to material distortion and fabrication induced defects

Transmission filters are very similar in performance to reflective filters with the exception of high sensitivity to wavelength errors. This may in extreme cases lead to a complete loss of signal power (infinite insertion loss) due to excessive angular dispersion in the filter.

Finally, the use of multiple grating reflection filters is discussed. Multiple transmission filters on the account of their sensitivity to wavelength tolerances will not be considered. The wavelength selective element in multiple grating reflection filter consists of a superposition of several simple reflection gratings, with each simple grating component selecting one channel. A possible configuration for a multiple grating reflection filter is shown in Figure 5.10a. To minimize path length the devices are used at $\phi = \pi/4$ inclination. In external arrangement the grating is similar to angularly dispersive devices with the difference that the spatial position of each output beam can be adjusted independently.

Another possible configuration of a multiple reflection grating is shown in Figure 5.10b. The grating is used at normal incidence, at which the angular sensitivity of the filter is minimum and the wavelength sensitivity is maximum. The advantage of this configuration is that the characteristics of the filter will be essentially polarization independent. Also, notice the use of a single collimating lens.

The fabrication and the performance of a multiple grating, in principle, similar to that shown in Figure 5.10a, was described recently by Livanos et al.[13] The device is described in section 5.4. A multiple grating device similar to that shown in Figure 10b so far has not been realized.

In concluding this section the possible problematic areas in the fabrication and performance of thick multiple gratings should be mentioned. Firstly, it is expected that deviations from the ideally assumed variation in the refractive index or grating period will lead to an increase in insertion loss and crosstalk. Experiments on actual gratings should quantify the effects of these imperfections. Secondly, due to the lack of available materials for the fabrication of multiple gratings a delay in the implementation of various proposed gratings is expected. Further research in this area should bring the required progress.

a)

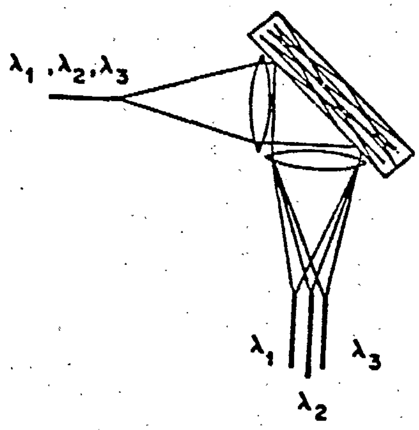

b)

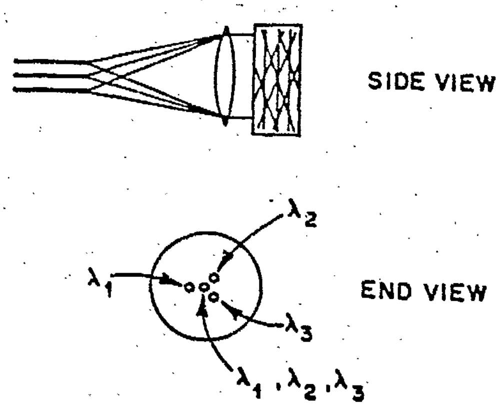

Figure 5.10 Multiplexers using multiple-grating thick reflection filters

5.3.3 Prototype design of a three channel WDM system

A summary of the result for the design of various multiplexers for a three channel WDM system is shown in Table 5.3.[4] The multiplexer dimensions were calculated by assuming a center wavelength of 820 nm, a channel separation $\Delta\lambda$= 25 nm and a wavelength tolerance of $\Delta\lambda = \pm$ 25 nm. The input and output are through fibers with NA = 0.2 and core diameter of d = 55 μm. The crosstalk and the insertion loss are specified to be less than 10 dB.

5.4 EXPERIMENTAL MULTIPLEXING DEVICES

In this section a brief description is given of several recently fabricated multiplexing and demultiplexing devices. The list is by no mean exhaustive and should be rather considered as an indication of the present day state-of-the-art technology.

A prism,[14] a simple grating,[15] and a chirped grating[13] (multiple grating) all used in a demultiplexer configuration are described.

The performance of cylindrical lenses (GRIN rod lenses) in the role of multiplexers is also described. The characteristics of a multifiber combiner were given earlier.[3]

The use of CdS prisms for demultiplexing of optical signals was demonstrated by Ishio and Miki[16] using LED's and by Sugimoto[6] et al. using lasers. In the first experiment three LED's at 784 nm, 825nm and 858 nm served as light sources. The multiplexing circuit consisted of an objective lens and three microcylindrical lenses (diameter = 1.5 mm). The insertion loss of the multiplexer was 12 dB. The demultiplexing circuit consisted of a prism and two objective lenses. The insertion loss of the demultiplexer was 7 dB. The prism size was about 1 cm.

In the second experiment the wavelengths of the laser sources were 805nm, 823 nm, and 863 nm. The multiplexer, which was of the type shown in Figure 5.3, could multiplex up to four input beams and consisted of four input GRIN rod lenses to collimate the input beams and one output lens to combine and launch the collimated beams into the output fiber. A CdS prism served as a demultiplexer. The insertion loss of the multiplexer and that of the demultiplexer was about 3 dB.

Microoptics devices particularly suitable for multiplexing and demultiplexing 2 channels have recently been described by Kobayashi et al.[2] The devices utilize GRIN rod lenses as basic building components. Multiplexing-demultiplexing is is achieved with the aid of wavelength selective mirrors inserted between the two facets of focusing rods. (See figure 5.11) The insertion loss of a prototype demultiplex device was 2.3 dB @ 822 nm from which 1.6 dB was attributed to filter reflection loss. Isolations of 24 dB and 28 dB were measured for wavelengths 30 nm above and below the center wavelength. The same device could also be used as a multiplexer.

TABLE 5.3 Summary of Results for Multiplexers Using Various Types of Wavelength-Sensitive Elements

Wavelength sensitive elements	Number of elements: Wavelength sensitive elements	Collimators	Spacers	Approximate overall dimensions (cm)	Polarization sensitivity	Cross-talk	Comments
Prism (Littrow Mount)	1	1	1	1x1x1.5 (Depends on materials)	Weak	Low	Practical devices with available materials
Blazed plane reflection grating	1	1	1	0.2 diam x 1	Weak	Low	Practical device with currently available materials
Simple thick reflection grating	2	4	4	5x3x1/2	Strong	High	Materials not currently available. Requires multiple elements
Multiple thick reflection grating	1	1	0	0.1 diam x 1/2	Weak	Med.	Materials not readily available
Simple thick transmission grating	2	4	4	-	Strong	High	Too sensitive to wavelength errors. Materials not currently available. Requires multiple elements.

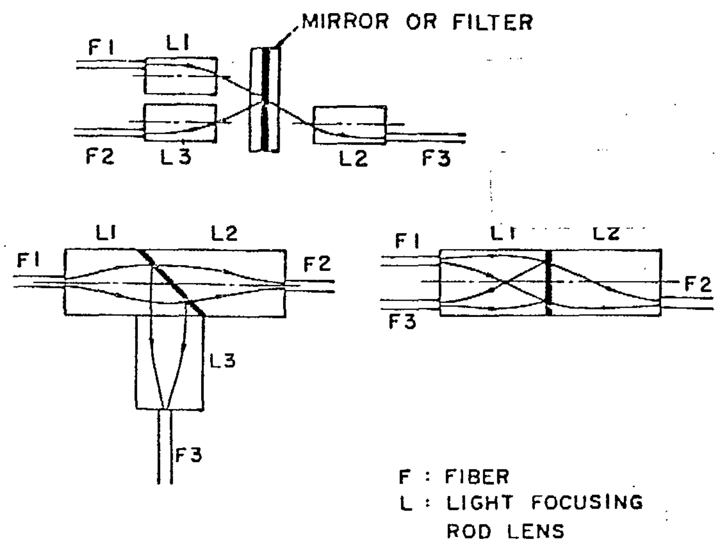

Figure 5.11 Multiplexers using GRIN rod lenses with filters or mirors

Tomlinson and Aumiller[15] recently reported the performance of a two channel optical multiplexer which was constructed using commercially available components (Figure 5.12). The device is reciprocal and could operate either as a multiplexer or as a demultiplexer. Its performance was demonstrated in a more demanding demultiplexer form. The demultiplexer consisted of a blazed plane reflection grating and of a single GRIN-rod lens. The wavelength spacing of the two channels was 27 nm, the insertion losses was less than 2.4 dB and the crosstalk was less than 30 dB. Optimized versions of the device should be capable of providing at least 4 channels, with still lower insertion losses in a package 1-2 cm long and 2-4 mm in diameter.

A performance of a wavelength selective beam splitter was recently described by Livanos et al.[13] The filter was realized by a fabrication of a chirped (variable period) grating in an optical waveguide. (Figure 5.13) The beam splitter could demultiplex a signal travelling in a fiber and send each wavelength component to a different fiber or detector. Reversing the direction of beams the device could also operate as a multiplexer. The principles of operation of this multiple grating device were reviewed earlier in Section 5.3. Efficient demultiplexing was demonstrated by launching the tunable output beam of a CW dye laser into the waveguide and by observing the locations of reflection of different wavelengths as the laser was tuned between 600-630 nm. No loss figures were given. The use of chirped gratings has also been reported for the realization of broad band optical filters in thin film waveguides. Bandwidths of 30 nm and 150 nm and reflectivities of 18% and 40% respectively were reported.[16]

5.5 SUMMARY

The technical demonstrations of experimental WDM systems, and the recent developments in the area of mux/demux fabrication show that WDM appears to be a feasible technique for increasing the capacity of a fiber optics based transmission medium. Further work should determine the practicability of proposed wavelength sensitive elements particularly in concern with field applications. The question of cost and mass production will also play an important role in future system developments.

Additional study is required for understanding the characteristics of multiplexers fabricated under the limitations of present day technology. Limitations imposed by aberrations in optical systems should also be studied.

It is also expected that the desired ruggedness and the required resistance against mechanical shocks and aberrations will place severe constraints on the assembly and the alignment geometry of the multiplexer. In this context the role of immersed designs becomes apparent. Immersed designs in forms of epoxies offer an advantage in that the whole assembly can be cemented. A reduction in crosstalk and system losses from internal reflections at dielectric interfaces is also expected.

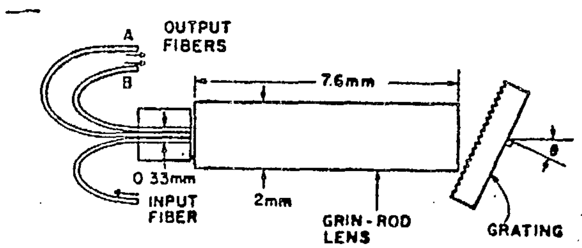

Figure 5.12 GRIN rod lens and grating as multiplexer/demultiplexer

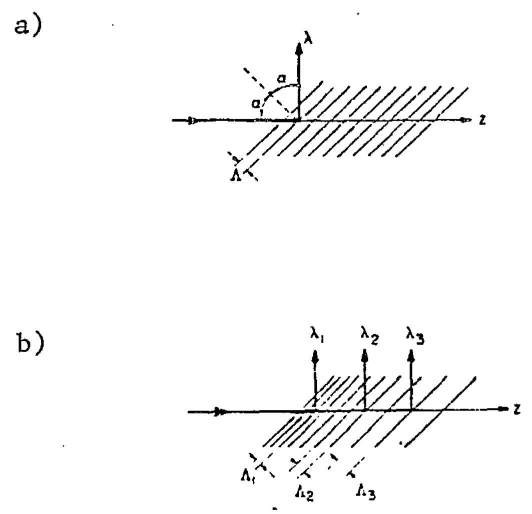

Figure 5.13 Beamsplitting in dielectric waveguides
a) constant grating period
b) chirped grating

In conclusion, there appear to be no internally imposed limitations on the fabrication of multiplexers for WDM applications. Presently GRIN rods,[2] multifiber combiners,[3] prisms[6, 14] and gratings[15] can serve as multiplexers. The latter two devices will also fulfill the role of demultiplexers. Although the feasibility of a thick diffraction grating as a multiplexer has already been demonstrated,[13] the device is polarization dependent and further work is required to establish the degree of its usefulness.

5.6 REFERENCES

5.1 T. Uchida, M. Furukawa, I. Kitano, K. Koizumi and H. Matsumura, IEEE J. Quantum Elect. QE-6, 606 (1970)

5.2 K. Kobayashi, R. Ishikawa, K. Minemura, S. Sugimoto, IOOC, 1977, Japan, B11-3

5.3 K.O. Hill, B.S. Kawasaki, and D.C. Johnson, Applied Physics Letters 31, 740, (1977)

5.4 W.J. Tomlinson, Appl. Opt. 16, 2190 (1977)

5.5 S. Hata, Opt. Q. Elect. 9, 265 (1977)

5.6 S. Sugimoto, K. Minemura, K. Kobayashi, M. Seki, M. Shikada, A. Ueki, T. Yanase, T. Miki, IOOC, 1977, Japan, C7-4; Elect. Letters 13, 680 (1977)

5.7 M. Born and E. Wolf, Principles of Optics, Pergamon Press, 1959.

5.8 Bausch and Lomb, Diffraction Grating Handbook.

5.9 Jobin-Yvon Optical Systems, Diffraction Gratings, Ruled and Holographic.

5.10 PTR Optics Corp. Diffraction Grating Catalog.

5.11 D. Marcuse, Light Transmission Optics, Van Nostrand, 1972.

5.12 H. Kogelnik, Bell Syst. Tech. J. 48, 2909 (1969).

5.13 A.C. Livanos, A Katzir, A. Yariv and C.S. Hong, Applied Physics Letters 30, 519 (1977).

5.14 H. Ishio and T. Miki, IOOC, 1977, Japan, C7-3.

5.15 W.J. Tomlinson and G.D. Aumiller, Applied Physics Letters 31, 169 (1977).

5.16 C.S. Hong, J.B. Shellan, A.C. Livanos, A. Yariv and A. Katzir, Applied Physics Letters 31, 276 (1977)

6. ANALYSIS OF A DISPERSIVE WDM DEMULTIPLEXER

6.1 INTRODUCTION AND SUMMARY

This chapter is a refinement of the analysis presented as Appendix B of Activity Report No. 5. Specifically, the analysis here incorporates the effects of lens aberrations and diffraction limitations on the performance of the demultiplexer.

The objective of this chapter and of the previous work is to predict the performance of a WDM demultiplexer in terms of the trade-offs between insertion loss, cross-talk between channels and the number of channels which can be multiplexed on one fibre.

The chapter begins by reviewing the properties and equations of diffraction gratings, especially blazed gratings, and incorporating the effects of diffraction limitations and of lens aberrations on the system resolution. As a specific example a demultiplexer with -60 dB crosstalk and 3 dB insertion loss is studied. It is found that 7 channels can be multiplexed in the optical band 800 - 900 nm, assuming spectrally stable light sources.

6.2 THE DIFFRACTION GRATING (References 6.1 and 6.2)

The most general form of the "grating equation" is:

$$k \lambda = c (\sin\theta_1 + \sin\theta_2) \tag{6.1}$$

where: k is the order of diffraction (integer number)
- λ the light wavelength
- c the groove spacing
- θ_1 the angle of incidence
- θ_2 the angle of diffraction

The basic equation fully describes the multiple diffraction behavior of a grating: a beam of wavelength λ and angle of incidence θ_1 is diffracted into a multiplicity of discrete beams leaving the grating at angles θ_2. To each integer value of k, there corresponds one diffracted beam.

It is important to note that equation 6.1 is independent of the groove shape. However, this shape greatly influences the distribution of the diffracted power among the various orders. Specifically, a triangular profile (called an "échelette" grating) can produce a high power concentration in the first order ($k = 1$). In this case, 6.1 becomes

$$\sin \theta_2 = \frac{\lambda}{c} - \sin \theta_1 \tag{6.2}$$

For the particular "blaze" wavelength

$$\lambda_B = 2\ c\ \sin\theta_1$$

equation 6.2 presents the possibility of having $\theta_2 = \theta_1$. At λ_B, the grating is said to be used in autocollimation. A grating so operated is also referred as being in the Littrow configuration. This mounting is attractive because of the good efficiency that occurs around λ_B. Figure 6.1 explains the behavior of a reflection grating, where 3 monochromatic beams (λ_1,λ_B and λ_2) are impinging at the same angle

Autocollimation arises at λ_B if groove spacing and incidence angle obey the relationship

$$c\ \sin\theta_1 = \frac{\lambda_B}{2} \tag{6.3}$$

Finally, the diffraction angle can be expressed in terms of: λ_B

$$\sin\theta_2 = \left(\frac{2\lambda}{\lambda_B} - 1\right) \sin\theta_1 \tag{6.4}$$

The anticipated system looks as shown in Figure 6.2. No assumption is made about the type of detectors. These are modelled as light sensitive surfaces behind an aperture. In practice, fibers may be attached to actual detectors, and it will be their ends which define the detector aperture. Both detectors and transmission fiber are located in the same plane which is perpendicular to the optical axis of the lens, and at a distance f from the lens, where f is the lens focal length. Thus, it is necessary to tilt the grating slightly about an axis perpendicular to the direction of the grating, in order to avoid superimposing the input and output beams at the autocollimation blaze wavelength λ_B.

This mount is interesting, because it needs only one lens (or one lens system), which acts both as a collimator for the input and a focusing lens for the output. Notice the unit magnification of the optical system.

6.2.1 Free Spectral Range

Because of the various diffraction orders, radiations of different wavelengths can be diffracted at the same angle. It is easy to show that the range of wavelengths without any superposition effect is equal to the minimum wavelength emerging from the fiber. (This result is valid for a first order Littrow mount, i.e. k = 1 in equation 6.1).

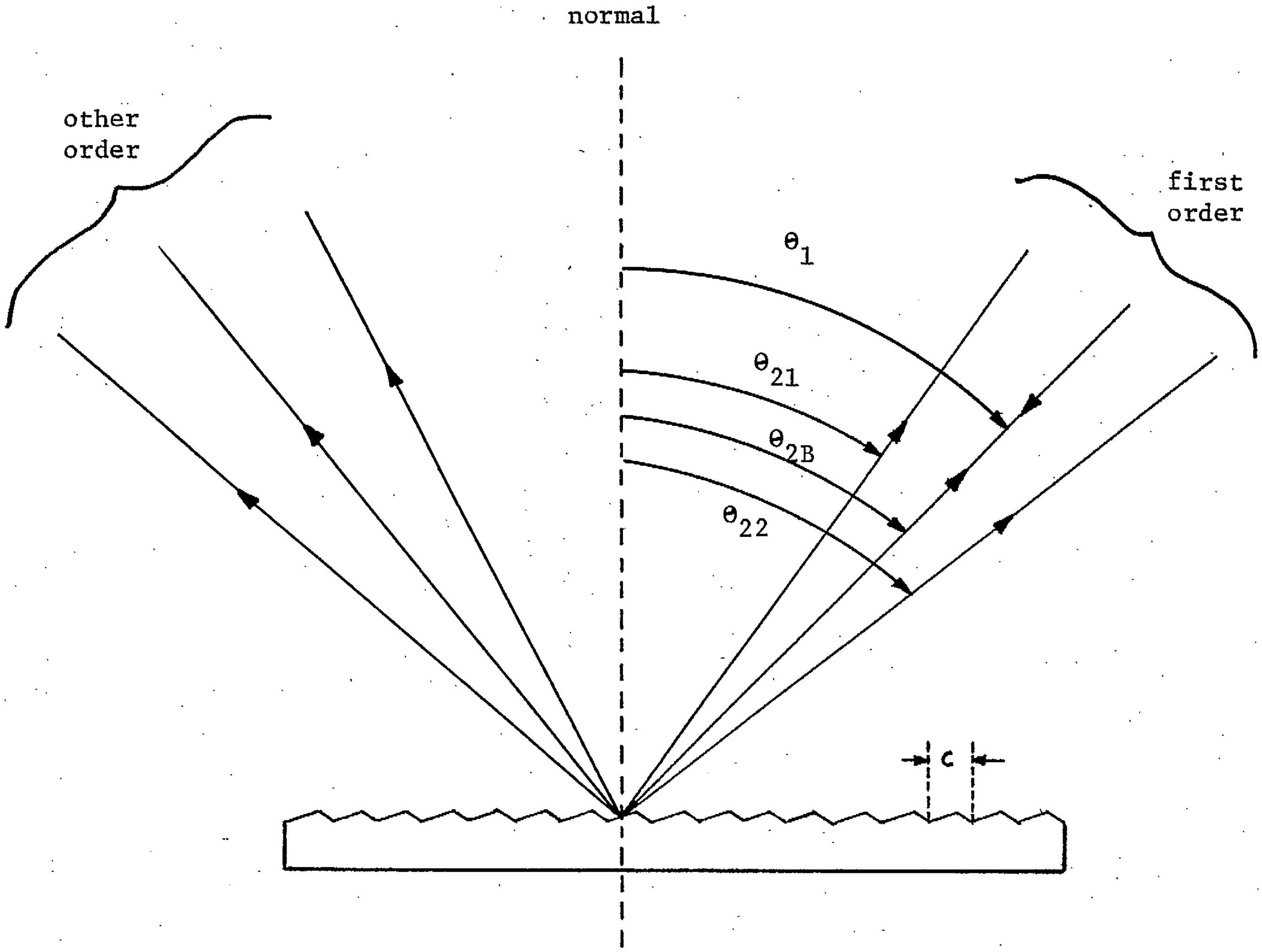

First order: wavelength	diffraction single
λ_B	$\theta_{2B} = \theta_1$
λ_1 ($< \lambda_B$)	θ_{21} ($< \theta_{2B}$)
λ_2 ($> \lambda_B$)	θ_{22} ($> \theta_{2B}$)

Figure 6.1. The effect of changing λ on the angle of diffraction, θ_2, for a fixed angle of incidence, θ_1.

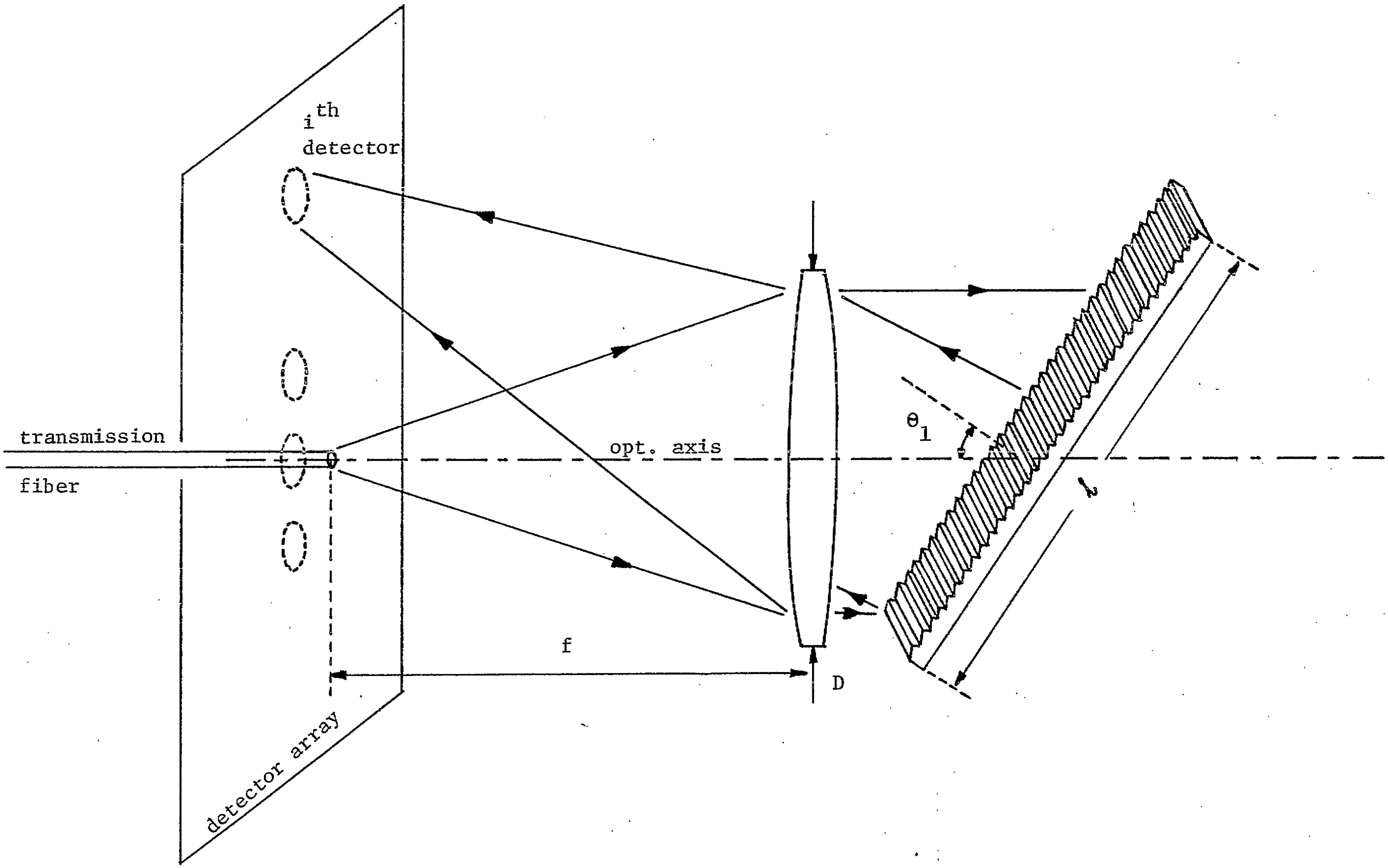

Figure 6.2. The WDM demultiplexer using a diffraction grating operating in autocollimation.

6.2.2 Angular Dispersion

The angular dispersion coefficient is given by $D_a = \frac{d\theta_2}{d\lambda}$. From grating equation 6.2,

$$D_a = \frac{1}{c \quad 1-(\frac{\lambda}{c} - \sin\theta_1)^2} \tag{6.5}$$

In autocollimation, $\theta_2 = \theta_1$ and the dispersion coefficient is

$$D_a(\lambda_B) = \frac{2 \tan\theta_1}{\lambda_B} \tag{6.6}$$

If f is the focal length of the lens, the corresponding linear dispersion coefficient is $D_l = f D_a$, for small values of D_a and small ranges of λ.

It follows from 6.6 that the grating dispersivity grows if the angle of incidence θ_1 grows. This increase in dispersivity, however, must be balanced against the effect of increasing θ_1 on lens aberrations, which can increase greatly at off-axis operation. If we call λ_M the farthest wavelength from λ_B, we can derive for the corresponding maximum off-axis angle Ω the approximate equation

$$\sin\Omega \simeq 2 \frac{(\lambda_B - \lambda_M)}{\lambda_B} \tan\theta_1 \tag{6.7}$$

valid for small Ω.

6.3 SYSTEM ANALYSIS

The scheme of analysis is as follows:

- Derivation of the equation for the spatial distribution of light imaged by the WDM demultiplexer; this analysis includes the effects of diffraction and lens aberrations.

- Computation of the number of optical sources which may be multiplexed within a given range in wavelength.

6.3.1 Image Equation of one WDM Channel

To simplify the drawing, Figure 6.3 defines the coordinate system which will be used in the analysis in terms of a transmission grating. However, the analysis applies to the reflection grating without any modification.

(x_p, x_d) are the cartesian coordinates at the fiber end, with the origin at the fiber center. Likewise, (y_p, y_d) are the coordinates in the detector plane. The fiber is assumed to be

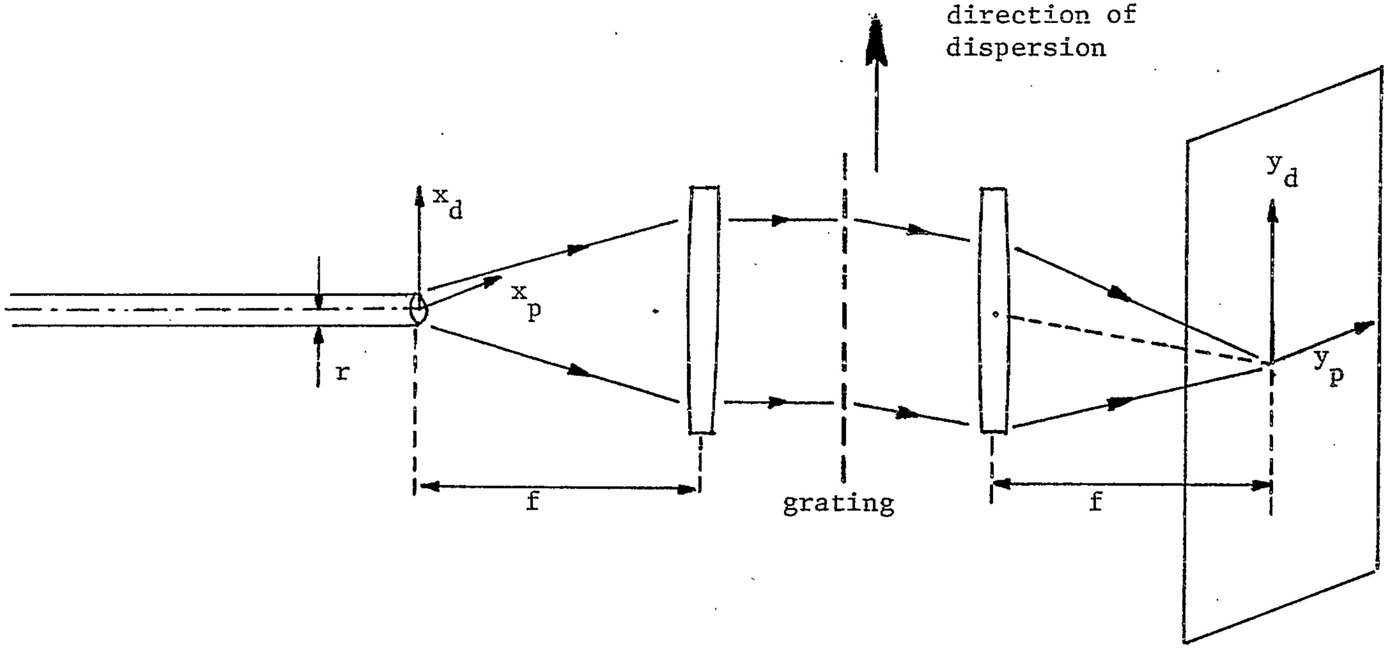

Figure 6.3. Coordinate system for analysis

illuminated by a single light source (laser diode, LD) of central wavelength λ_0. In this case, the origin in the y-plane coincides with the image by the demultiplexer of the fiber center illuminated by monochromatic light of wavelength λ_0. y_d and y_p are, respectively, parallel and perpendicular to the direction of dispersion dictated by the grating.

The spatial and spectral distributions of the fiber output are considered as independent. Thus, the light distribution at the output of the fiber, $0\,(x_p, x_d; \lambda)$, can be written

$$0\,(x_p, x_d; \lambda) = 0'\,(x_p, x_d)\ S(\lambda)$$

The spatial intensity variation $0'(x_p, x_d)$ may reasonably be modelled by a truncated gaussian distribution:

$$0'(x_p, x_d) = \begin{cases} A\, e^{-\frac{x_p^2}{2\sigma_x^2}}\, e^{-\frac{x_d^2}{2\sigma_x^2}} & \text{for } \sqrt{x_p^2 + x_d^2} \leq r \\ 0 & \text{elsewhere.} \end{cases} \tag{6.8}$$

The spectral density of the LD light is supposed to have a gaussian distribution in wavelength

$$S(\lambda) = B\, e^{-\frac{(\lambda - \lambda_0)^2}{2\sigma_\lambda^2}}$$

The computation of the image produced by such an optical object will be divided into two parts: the first is concerned with aberrations and diffraction, the second with dispersion.

The Effects of Aberrations and Diffraction on Resolution

In any optical system the resolution is limited by two factors - aberrations of lenses or other optical components and diffraction. Diffraction effects can be decreased by increasing the aperture of the system, while aberrations always increase with the aperture - for example, spherical aberrations increase as the fourth power of the aperture. In an optimum system the aperture is selected to minimize the point spread function of the system - the optical analogue of the impulse response function of electrical circuit analysis. This point spread function may be characterised by a gaussian:

$$I_a(y_p, y_d) = C\, e^{-\frac{y_p^2}{2\sigma_A^2}}\, e^{-\frac{y_d^2}{2\sigma_A^2}} \tag{6.9}$$

An electrical network is said to be time-invariant if its impulse response $h\,(t, \tau)$ depends only on the time difference $(t - \tau)$. In a similar fashion, a linear imaging system is said to be space-invariant or isoplanatic if its impulse response Ia $(y_p, y_d; x_p, x_d)$ depends only on the distances $(y_p - x_p)$ and $(y_d - x_d)$. In other words, the system is space-invariant if the image of a point-source object changes only in location, not in functional form, as the point source explores the object field. (see reference 6.3). In this case, a linear transfer function can be defined; the block-diagram is shown in Figure 6.4.

Thus, we can write the image due to diffraction and aberrations alone as a convolution integral, indicated by an *:

$$I\ (y_p, y_d) = O'\ (y_p, y_d) * Ia\ (y_p, y_d)$$

For O', the coordinates (x_p, x_d) have been replaced by (y_p, y_d) because a reflection system in autocollimation has unit magnification. For other systems, it would be necessary to write the image as $O'\ (ky_p, ky_d)$, where k describes the system magnification.

The Dispersive Effect

We now consider separately the effect on the image of the dispersion of the system, and the fact that the light distribution at the end of the fiber is not monochromatic. Though the coefficient of dispersion D_a is wavelength-dependent (equation 6.5), it is assumed to be constant within the narrow spectrum of a LD. This assumption will be justified through numerical values.

Thus, to the gaussian distribution of LD spectrum as a function of wavelength, there will correspond a gaussian distribution of light along the y_d dispersion axis. The LD having a standard deviation σ_λ, the resulting standard deviation on y_d - axis is

$$\sigma_{yd} = D_l\ \sigma_\lambda \qquad (6.10)$$

($D_l = D_a f$: linear dispersion, as defined in Section 6.2.2 above).

Figure 6.5 shows the block-diagram for dispersion. It follows that the light distribution of the image of a point source $\delta(x_p) \cdot \delta(x_d)$, of spectrum $S\ (\lambda)$, is given by

$$I_2\ (y_p, y_d) = K \cdot \delta\ (y_p)\ e^{-\frac{y_d^2}{2\sigma_{y_d}^2}} \qquad (6.11)$$

where K combines a constant to account for losses and a constant to preserve normalisation.

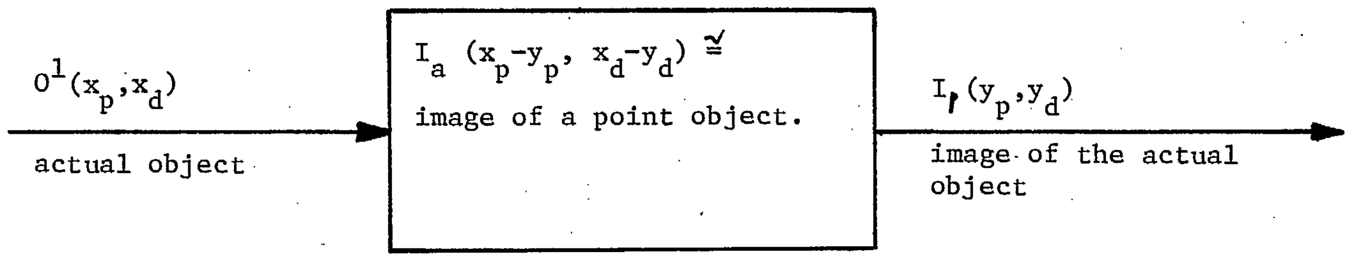

Figure 6.4. Block-diagram for aberration and diffraction.

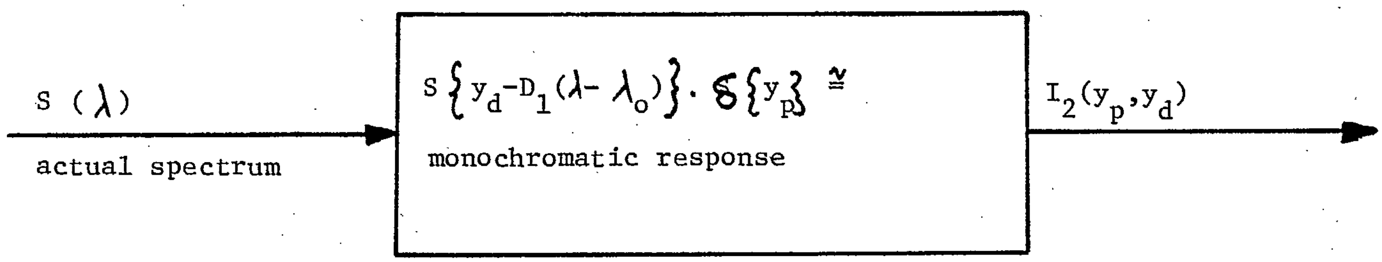

Figure 6.5. Block-diagram for dispersion

Block-Diagram of the System

From the above decomposition, we can now represent the system in a general block-diagram (Figure 6.6). The first block represents aberrations and diffraction; the second one represents dispersion. The image at the output of the WDM demultiplexer is the result of both these filters acting on the three-dimensional input, $O(x_p, x_d, \lambda)$: where the mapping of the third dimension, λ, on y_p and y_d is achieved by the filter function $I_2(y_p, y_d)$.

$$I(y_p, y_d) = O'(y_p, y_d) * I_a(y_p, y_d) * I_2(y_p, y_d) \qquad (6.12)$$

Equations 6.8, 6.9, 6.11 point out that each of the three functions to be convolved together is separable in the chosen coordinate system. This feature permits one to perform 6.12 independently along the y_p and y_d axes.

Image along the Dispersion Axis

The image along the dispersion axis consists of the convolution of 3 gaussians, one being truncated. The convolution of 2 gaussians is quickly performed, using the Laplace transform. It results in another gaussian, whose variance is the sum of the 2 initial variances:

$$I_a(y_d) * I_2(y_d) = C\, e^{-\frac{y_d^2}{2\sigma_a^2}} * K\, e^{-\frac{y_d^2}{2\sigma_{y_d}^2}}$$

$$= K_1\, e^{-\frac{y_d^2}{2(\sigma_a^2+\sigma_{y_d}^2)}} \qquad (6.13)$$

(Henceforth, multiplicative factors, such as K_1 above, will be chosen as unity. If necessary, we can always normalize the final results).

The next step is to convolve 6.13 with the truncated gaussian $O'(y_d)$:

$$I'(y_d) = \int_{-\infty}^{\infty} O'(z)\, \exp\left\{-\frac{(y_d - z)^2}{2(\sigma_a^2+\sigma_{y_d}^2)}\right\} dz$$

$$= \int_{-r}^{r} e^{-\frac{z^2}{2\sigma_x^2}} \cdot \exp\left\{-\frac{(y_d - z)^2}{2(\sigma_a^2+\sigma_{y_d}^2)}\right\} dz \qquad (6.14)$$

because $O'(y_d) \neq 0$ only when $-r < y_d < r$.

The evaluation of equation 6.14 was achieved in Appendix B of the Activity Report No. 5. The results were shown there to be:

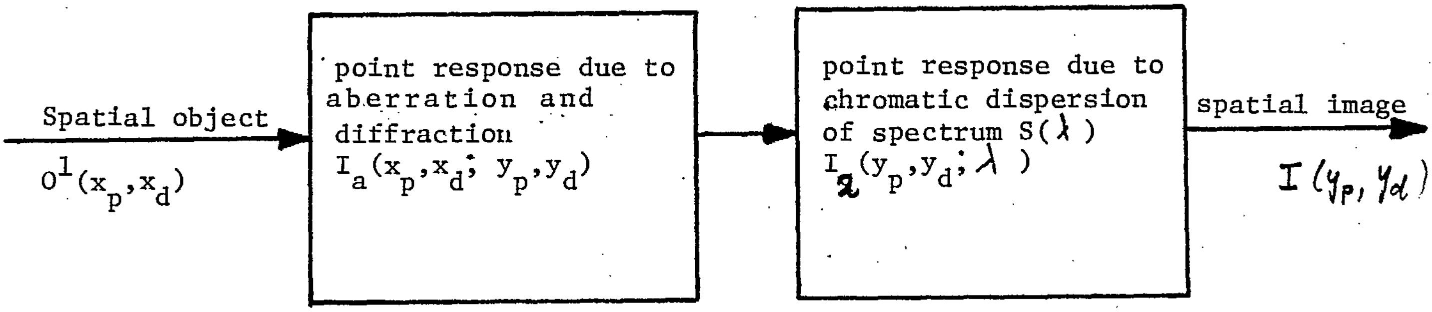

Figure 6.6. General block-diagram of the WDM demultiplexer.

$$I'(y_d) = \exp\left\{-\frac{y_d^2}{2(\sigma_a^2+\sigma_{y_d}^2+\sigma_x^2)}\right\}\left[\operatorname{erf}\left\{\frac{r\sqrt{\sigma_a^2+\sigma_{y_d}^2+\sigma_x^2}}{\sigma_x\sqrt{2(\sigma_a^2+\sigma_{y_d}^2)}} - \frac{\sigma_x \cdot y_d}{\sqrt{2(\sigma_a^2+\sigma_{y_d}^2)(\sigma_a^2+\sigma_{y_d}^2+\sigma_x^2)}}\right\}\right.$$

$$\left. + \operatorname{erf}\left\{\frac{r\sqrt{\sigma_a^2+\sigma_{y_d}^2+\sigma_x^2}}{\sigma_x\sqrt{2(\sigma_a^2+\sigma_{y_d}^2)}} + \frac{\sigma_x \cdot y_d}{\sqrt{2(\sigma_a^2+\sigma_{y_d}^2)(\sigma_a^2+\sigma_{y_d}^2+\sigma_x^2)}}\right\}\right] \qquad (6.15)$$

where erf is the error function, as normally defined.

Image along the Perpendicular Axis

The calculation to be performed is

$$I''(y_p) = O'(y_p) * Ia(y_p) * I_2(y_p) \qquad (6.16)$$

Because of no dispersion along this axis, we have a delta distribution for $I_2(y_p)$. (See equation 6.11). Now, this distribution has the general property

$$f(x) * \delta(x) = f(x)$$

By taking $f = O' * I_a$, (16) becomes

$$I''(y_p) = O'(y_p) * I_a(y_p),$$

corresponding to the convolution of 2 gaussians one of which is truncated:

$$I''(y_p) = \int_{-r}^{r} e^{-\frac{z^2}{2\sigma_x^2}} \; e^{-\frac{(y_d - z)^2}{2\sigma_a^2}} \, dz$$

As for equation 6.14. the result given in Activity Report No. 5 is:

$$I''(y_p) = e^{-\frac{y_p^2}{2(\sigma_a^2+\sigma_x^2)}}\left[\operatorname{erf}\left\{\frac{r\sqrt{\sigma_x^2+\sigma_a^2}}{\sqrt{2}\,\sigma_x\sigma_a} - \frac{\sigma_x\, y_p}{\sigma_a\sqrt{2(\sigma_x^2+\sigma_a^2)}}\right\}\right.$$

$$\left. + \operatorname{erf}\left\{\frac{r\sqrt{\sigma_x^2+\sigma_a^2}}{\sqrt{2}\,\sigma_x\sigma_a} + \frac{\sigma_x\, y_p}{\sigma_a\sqrt{2(\sigma_x^2+\sigma_a^2)}}\right\}\right] \qquad (6.17)$$

Finally, combining these results, the two-dimensional image is described by

$$I(y_p, y_d) = I'(y_d) \cdot I''(y_p)$$

where $I'(y_d)$ and $I''(y_p)$ are expressions (6.15) and (6.17).

6.3.2 Extension to the Case of Several Channels

At this stage, we possess an analytic expression for the image due to one optical channel alone, centered at wavelength λ_o. Now, the actual multiplex is formed of N different sources, centered at wavelengths λi (i = 1, ...N). Thus, we introduce a new terminology, and write the input light spectrum as

$$S(\lambda) = \sum_{i=1}^{N} B_i \, e^{\frac{-(\lambda-\lambda_i)^2}{2\sigma_{\lambda_i}^2}} \tag{6.18}$$

Figure 6.7 shows a schematic of the demultiplexer. The grating mounting is such that the N demultiplexed outputs are located symmetrically on each side of the lens optical axis, which is achieved by making the blaze wavelength, λ_B, correspond with the central wavelength of the series of sources.

6.3.3 Crosstalk Calculations

Referring to Figure 6.7 the i^{th} detector will be centered at y_i, i.e. on the image of the centre of the fiber illuminated by the i^{th} light source (emitting around λi). The desired signal on the i^{th} detector is that due to the i^{th} source; the undesired is that due to all other sources.

Crosstalk calculations depend on the choice of "windows" in front of each detector. Because the image does not present a circular symmetry, circular windows are not necessarily optimum; besides, they create difficulties for analytic integration as were encountered in Activity Report No. 5. So, we suppose the power of each channel is collected through a square aperture of side d. The problem is to find how large the spacing between two adjacent detectors h (along y_d) must be, for a given crosstalk figure and for a given value of d. The value of d, as discussed below, is determined by the insertion loss which can be tolerated. Knowledge of h will enable us to evaluate the maximum number of channels which may be multiplexed with the desired crosstalk performance.

Insertion Loss

The demultiplexing device involves inherent optical loss, due to lens reflectance and efficiency of the grating. Once we possess figures for these losses, we can compute the side d of the aperture which will provide the prescribed insertion loss. It will be shown later that improved performance can be achieved with a slit aperture of width d in the direction of dispersion, but extending further in the perpendicular direction. Such slits have identical crosstalk performance to the square apertures, but less insertion loss. For the moment, though, calculations are presented for the square aperture.

Crosstalk as a Function of Detector Spacing

Once the aperture size d is determined, we can deal with crosstalk as a function of the detector spacing h.

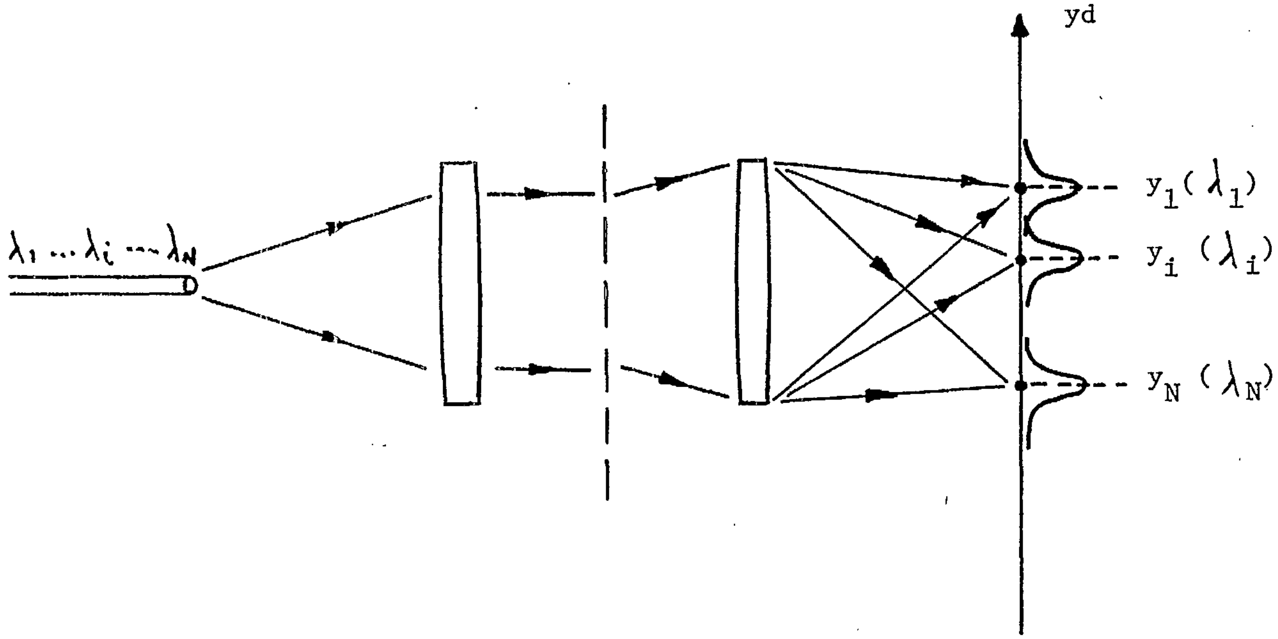

Figure 6.7. Schematic of the detector location, showing the light distribution due to each channel.

The equation for the desired signal power incident on the i^{th} detector through the aperture is:

$$P_s = \int_{-\frac{d}{2}}^{\frac{d}{2}} \int_{-\frac{d}{2}}^{\frac{d}{2}} I_{\lambda_i}(y_p, y_d)\, dy_p\, dy_d = \int_{-\frac{d}{2}}^{\frac{d}{2}} I'_{\lambda_i}(y_d)\, dy_d \cdot \int_{-\frac{d}{2}}^{\frac{d}{2}} I''_{\lambda_i}(y_p)\, dy_p \tag{6.19}$$

where index λ_i signifies that only contributions from the i^{th} source are included. For equation 6.19, the origin of the (y_p, y_d) coordinates is located at the image of the point source at the origin of the (x_p, x_d) plane, with monochromatic illumination λi (corresponding to the LD central wavelength).

It will be assumed that the only significant crosstalk comes from the light destined for the 2 adjacent detectors at y_{i+1}, y_{i-1}. Further, it will be assumed that all light sources (equation 6.18 have the same spectral width $\sigma\lambda_i = \sigma\lambda$, and the same level $B_i = B$. The latter assumption can be changed without causing basic alterations to the calculations.

The distribution of light power in the (y_p, y_d) plane due to $i \pm 1^{th}$ channel is:

$$I_{\lambda_{i\pm 1}}(y_p, y_d) = I''_{\lambda_i}(y_p) \cdot I'_{\lambda_i}(y_d \pm h)$$

Crosstalk from $i + 1^{th}$ channel into i^{th} channel becomes (see Figure 6.8).

$$P_{cr} = \int_{-\frac{d}{2}}^{\frac{d}{2}} I''_{\lambda_i}(y_p)\, dy_p \cdot \int_{-\frac{d}{2}}^{\frac{d}{2}} I'_{\lambda_i}(y_d - h)\, dy_d$$

Now,

$$\int_{-\frac{d}{2}}^{\frac{d}{2}} I'_{\lambda_i}(y_d - h)\, dy_d = \int_{-\frac{d}{2}-h}^{\frac{d}{2}-h} I'_{\lambda_i}(y_d)\, dy_d = \int_{h-\frac{d}{2}}^{h+\frac{d}{2}} I'_{\lambda_i}(y_d)\, dy_d$$

because $I'_{\lambda i}(y_d)$ is an even function by symmetry.

So,

$$P_{cr} = \int_{-\frac{d}{2}}^{\frac{d}{2}} I''_{\lambda_i}(y_p)\, dy_p \cdot \int_{h-\frac{d}{2}}^{h+\frac{d}{2}} I'_{\lambda_i}(y_d)\, dy_d \tag{6.20}$$

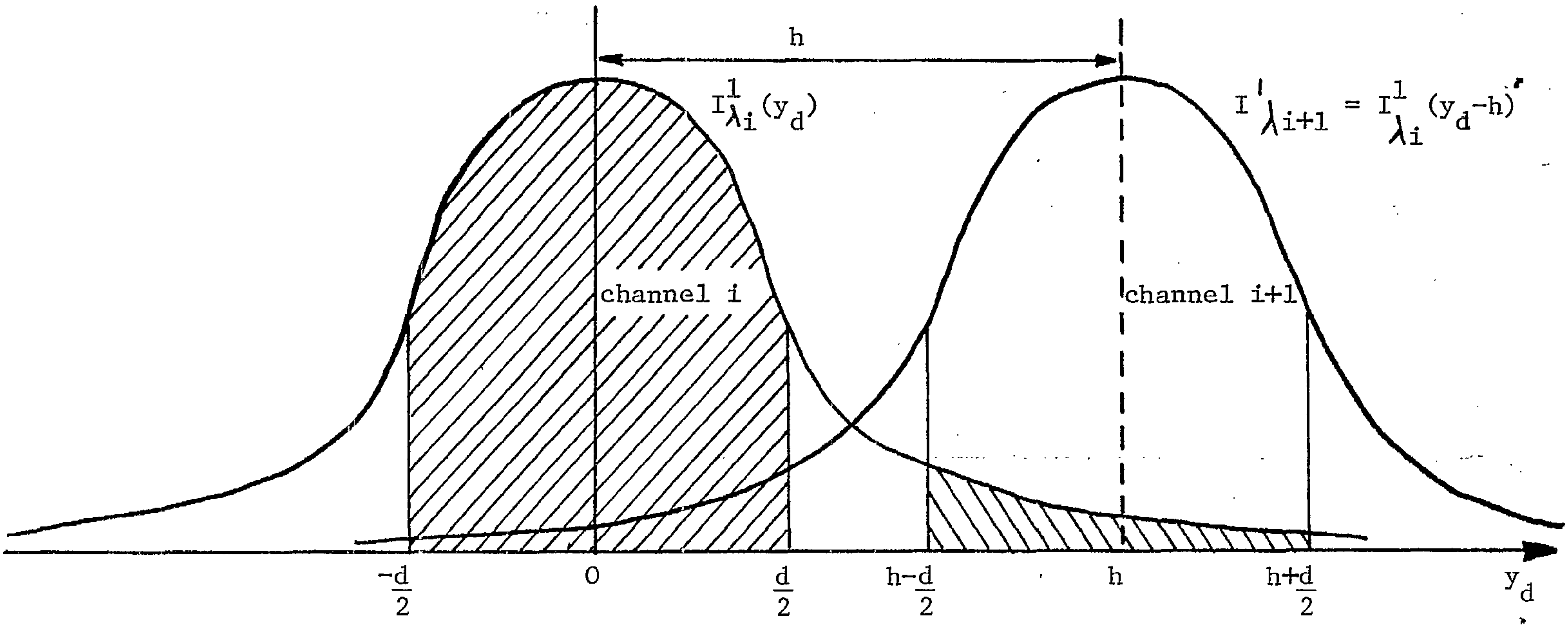

Figure 6.8. Illustration of light distribution for crosstalk calculations. The two hatched areas are respectively the desired signal on the ith detector and the undesired signal from the i th channel to (i+1)th channel.

Consequently, the crosstalk figure, as a ratio of crosstalk due to the two $i \pm 1^{th}$ channels to the desired i^{th} signal, is characterized by twice the ratio of equation 6.20 to equation 6.19:

$$\frac{P_{cr}}{P_s} = 2\,\frac{\int_{-\frac{d}{2}}^{\frac{d}{2}} I''_{\lambda_i}(y_p)\,dy_p \int_{h-\frac{d}{2}}^{h+\frac{d}{2}} I'_{\lambda_i}(y_d)\,dy_d}{\int_{-\frac{d}{2}}^{\frac{d}{2}} I''_{\lambda_i}(y_p)\,dy_p \int_{-\frac{d}{2}}^{\frac{d}{2}} I'_{\lambda_i}(y_d)\,dy_d} = \frac{\int_{h-\frac{d}{2}}^{h+\frac{d}{2}} I'_{\lambda_i}(y_d)\,dy_d}{\int_{0}^{\frac{d}{2}} I'_{\lambda_i}(y_d)\,dy_d} \qquad (6.21)$$

Note that by using a rectangular aperture this equation is significantly simplified in comparison with that used in Activity Report No. 5.

Figure 6.8 clarifies the above result.

6.3.4 Number of Channels which may be Multiplexed

The next step is to infer from 6.21 the value of spacing h which allows one to keep crosstalk below the desired level. Finally, it is easy to deduce the number of multiplexable channels: roughly, it is the total linear dispersion tolerated (related to lens aberrations) divided by the spacing h between two adjacent detectors.

6.4 NUMERICAL EXAMPLE

6.4.1 Basic Assumptions

For the sake of a numerical example, we shall deal with typical fibers, with the following features:

- numerical aperture N.A. = 0.2
- core radius r = 50 μm

For narrow emission bandwidth, light sources are assumed to be laser diodes, having a spectral bandwidth $\Delta\lambda$ = 3 nm. We decide to consider light within the band λ = 800 nm to λ = 900 nm, compatible with the low absorption region of silica fibers, and with GaAs technnlogy.

6.4.2 Numerical Values for the Grating

It is reasonable to select the autocollimation wavelength in the middle of the band of interest, i.e. λ = 850 nm. The grating equation is completely defined if groove spacing c and incidence angle θ_1 are known. From 6.3, these 2 parameters are connected by

$$c \cdot \sin\theta_1 = 425 \text{ nm} \qquad (6.22)$$

c and θ_1 are chosen on the basis of the following criteria: from 6.7, θ_1 must be limited in magnitude because of lens aberrations due to off-axis diffraction angle. As to c, excessively small values must be avoided: they would result in the price increasing because of the need for high precision in manufacture.

A full treatment of lens aberrations is quite beyond the scope of this report. The interested reader is referred to reference 6.8. Some simplifying treatments are possible, though, and these are used here. In optics catalogues, mention is made of computer-optimized lenses, where the aberrations remain virtually constant up to an off-axis angle $\Omega = 3°$. Applying this figure to the extrema values 800 and 900 nm, 6.8 produces the upper limit:

$$\theta_1 < 24°$$

From 6.22; the corresponding groove density is

$$n < 957 \ \frac{\text{grooves}}{\text{mm}}$$

This order of magnitude is convenient, because grating catalogues speak of constant prices for classically ruled replica gratings up to about 800 grooves/mm. Above this value, prices increase with groove density. In brief, we select the parameters as:

$$\theta_1 = 20° \qquad c = 1.242\ \mu\text{m} \quad (n = 805\ \frac{\text{grooves}}{\text{mm}})$$

From theory, we have a free spectral range of 800 nm, which is sufficient since we only need 100 nm. (Future systems with light sources at around 1.2 μm may, however, profit from the full spectral range).

6.4.3 Parameters for Image Evaluation

At $\lambda_B = 850$ nm, the dispersion coefficient is given by 6.6:

$$D_a = 8.56 \times 10^{-4} \ \frac{\text{rad}}{\text{nm}}$$

In section 6.3, we supposed D_a = const. for a given LD. In fact, the inaccuracy of this assumption is less than 0.1% if the LD bandwidth is only $\Delta\lambda = 3$ nm.

For the spatial distribution 6.8 of the fiber output, we assume a standard deviation $\sigma_x = r/2 = 25\ \mu\text{m}$ for a first numerical example. This parameter is liable to modification as a result of experimental measurements.

Lens aberrations figures are based on the use of computer-optimized lenses. A conservative interpretation of figures given in reference 6.4 leads one to an angular spot radius of the image of a point source given by:

$$\phi = 2.3\ 10^{-3}\,\mathrm{rad} \tag{6.23}$$

This radius is a result of the combination of diffraction and aberrations. It needs further investigation.

The last parameter to consider is the lens local length f, whose role in the system is secondary. Specifically, it does not influence the magnification, which is unity. The only criterion for choosing f is the efficiency of coupling light from the fiber. For maximum efficiency the "F-number" of the lens must be no greater than

$$F = \frac{f}{D} = \frac{1}{2\ \mathrm{N.A.}} = 2.5$$

where N.A. is the NA of the fiber, D is the lens diameter. We choose arbitrarily f = 26 mm, and hence D should be no less than about 10 mm. These figures would give an acceptably small device, while still using easily obtainable lenses.

Having chosen f, the standard deviation due to aberrations and diffraction may now be written as

$$\sigma_a = \phi \cdot f = 60\ \mu m$$

for the above lens and diffraction grating.

In order for the full bandwidth at half maximum power of the LD to be $\Delta\lambda = 3$ nm, the gaussian spectrum must have a standard deviation of

$$\sigma_l = \frac{\Delta\lambda}{2\sqrt{2\ln 2}} = 1.27\ nm$$

From 6.10, the dispersion is characterized by

$$\sigma_{yd} = D_a \cdot f \cdot \sigma\lambda = 28.26\ \mu m$$

As to the grating size, we can match it with the lens size. Thus, taking account of the projection of the inclined grating (see Figure 6.2, the side of the square is about

$$1 = \frac{D}{\cos\theta_1} = 11\ mm$$

In brief, the parameters relevant to image evaluation (equations 6.15 and 6.17) are

$r = 50\ \mu m$
$\sigma x = 25\ \mu m$
$\sigma a = 60\ \mu m$
$\sigma yd = 28.26\ \mu m$

6.4.4 Approximations

At this stage, we have an analytical expression for the demultiplexed output associated with one LD channel. As shown, crosstalk calculations imply integrations of the expressions 6.15 and 6.17. We were not able to find an analytical expression for these integrals, so it would be necessary to use numerical methods for their evaluation. It is, however, preferable to deal with analytical approximations of the exact functions, if realistic approximations can be found. Two principal facts motivate that decision: firstly, the above calculations on the system are based on some assumptions (various gaussian distributions for simplicity). Thus, very precise calculations would not be consistent with these rough approximations. Secondly, some parameters are estimations, for lack of better information. So, each variation of a parameter would imply new numerical integrations. As a result, computer expenditures could be significant.

Equations 6.15, 6.17 and their respective approximations have been traced on the same sheet (see Figures 6.9 and 6.10). In both cases, the approximation involved replaces the factor $\left[\mathrm{erf}\{\ \} + \mathrm{erf}\{\ \}\right]$ by a factor of unity. As a result, 6.15 and 6.17 become simple gaussians. (It is easy to see that this corresponds to the case of a non-truncated gaussian for $0'$ (x_p, x_d). In other words, the smaller σx is with respect to the radius, r, the more correct is the approximation). In our case, we have $x = r/2$. A glance at the curves obtained proves the merits of the approximation. Notice that the larger the aberrations and the wider the LD spectrum is, the smaller the error in using this approximation becomes. (Truncation effects tend to be masked by the other effects).

6.4.5 Numerical Values for Insertion Loss

With appropriate antireflection coatings, the reflectance of the lens can easily be limited to 2%, i.e. 98% efficiency (see reference 6.4). Because light crosses the lens twice, the efficiency figure is

$$0.98^2 = 96\%$$

Concerning the grating, figures of practical efficiency are given in reference 6.5. It is interesting to notice that a "special

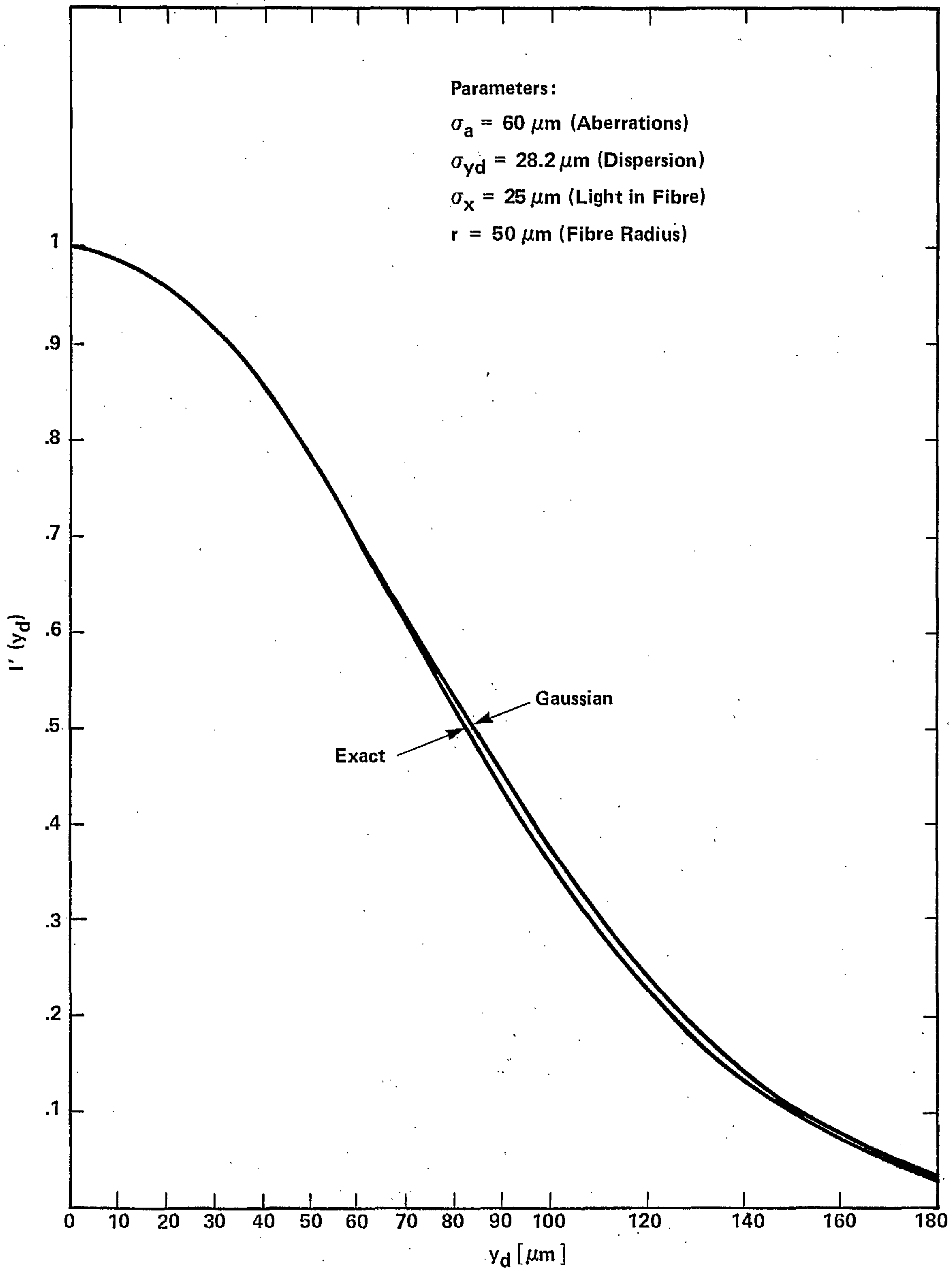

Figure 6.9 Approximation of $I'(y_d)$

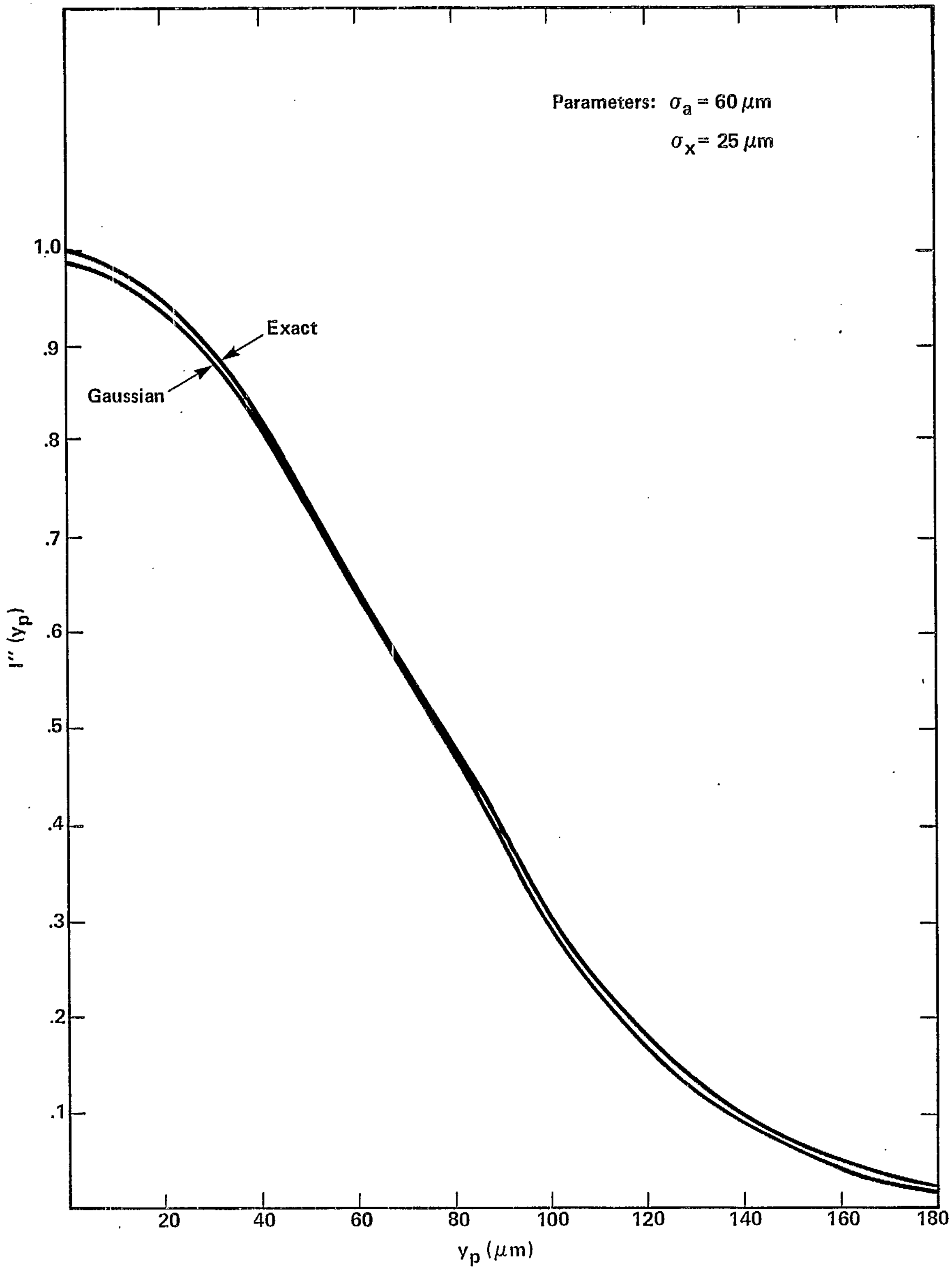

Figure 6.10 Approximation for $I''(y_p)$

low anomaly region" happens between 18° and 22° blaze angle, compared with the choice $\theta_1 = 20°$. With optimal groove shape, we can consider an absolute efficiency near to 80%. So, the inherent efficiency is given by the product

$$0.96 \times 0.8 = 77\%$$

To provide a basis for calculations, we impose a requirement that the total insertion loss should not exceed 3 dB, i.e. 50% optical efficiency is required. This determines the size d of the detector window: the squared aperture must collect

$$\frac{0.50}{0.77} = 65\%$$

of the output light.

Using the approximation discussed above, $I'(y_d)$ and $I''(y_p)$ take the form:

$$I'(yd) = \frac{1}{\sqrt{2\pi}\,\sigma_1} e^{-\frac{y_d^2}{2\sigma_1^2}}, \text{ where } \sigma_1^2 = \sigma_a^2 + \sigma_{y_d}^2 + \sigma_x^2 \quad (6.24)$$

$$I'(yd) = \frac{1}{\sqrt{2\pi}\,\sigma_2} e^{-\frac{y_p^2}{2\sigma_2^2}}, \text{ where } \sigma_2^2 = \sigma_a^2 + \sigma_x^2 \quad (6.25)$$

these functions are normalized, i.e.

$$\int_{-\infty}^{\infty} I'(y_d)\, dy_d = 1$$

$$\int_{-\infty}^{\infty} I''(y_p)\, dy_p = 1$$

We have to find $\frac{d}{2}$, so that

$$\int_{-\frac{d}{2}}^{\frac{d}{2}} I'(y_d)\, dy_d \cdot \int_{-\frac{d}{2}}^{\frac{d}{2}} I''(y_p)\, dy_p = 0.65$$

or:

$$2\int_0^{\frac{d}{2}} \frac{1}{\sqrt{2\pi}\,\sigma_1} e^{-\frac{y_d^2}{2\sigma_1^2}}\, dy_d \cdot 2\int_0^{\frac{d}{2}} \frac{1}{\sqrt{2\pi}\,\sigma_2} e^{-\frac{y_p^2}{2\sigma_2^2}}\, dy_p = 0.65 \quad (6.26)$$

Putting

$$z_1 = \frac{y_d}{\sqrt{2}\,\sigma_1} \qquad (dy_d = \sqrt{2}\,\sigma_1\, dz_1)$$

and: $$Z_2 = \frac{y_p}{\sqrt{2}\,\sigma_2} \qquad (dy_p = \sqrt{2}\,\sigma_2\, dZ_2)$$

6.26 becomes
$$\frac{4}{\pi} \int_0^{\frac{d}{2\sqrt{2}\sigma_1}} e^{-Z_1^2}\, dZ_1 \int_0^{\frac{d}{2\sqrt{2}\sigma_2}} e^{-Z_2^2}\, dZ_2 = 0.65$$

Now, by definition of the error function,
$$erf(u) = \frac{2}{\sqrt{u}} \int_0^u e^{-t^2} dt$$

So, we obtain the following equation for choosing $\frac{d}{2}$:
$$erf\left(\frac{d}{2\sqrt{2}\sigma_1}\right) erf\left(\frac{d}{2\sqrt{2}\sigma_2}\right) = 0.65$$

With the parameters defined in section 6.4.3, the equality is verified (from numerical tables) for

$$\frac{d}{2} \cong 90\ \mu m.$$

Until now, a squared window of side d was considered. From equation 6.21, it is interesting to notice that the crosstalk does not depend on the aperture width along the axis y_d, perpendicular to the dispersion axis y_d: (though this width affects the insertion (loss). Thus, it is possible to choose an aperture width greater than d along y_p. (In the limit, the window could become a slit perpendicular to the dispersion axis). While the crosstalk performance would not be degraded, the insertion loss would decrease.

6.4.6 Channel Spacing, and Number of Channels

From 6.21, 6.24, and the definition of the error function, the crosstalk is written as:

$$\frac{P_{cr}}{P_s} = \frac{erf\left(\frac{h+\frac{d}{2}}{\sqrt{2}\sigma_1}\right) - erf\left(\frac{h-\frac{d}{2}}{\sqrt{2}\sigma_1}\right)}{erf\left(\frac{d}{2\sqrt{2}\sigma_1}\right)}.$$

The final form is in terms of electrical dB of crosstalk:

$$C_{r\,(dB\ elect.)} = 20 \log\left[\frac{erf\left(\frac{h+\frac{d}{2}}{\sqrt{2}\sigma_1}\right) - erf\left(\frac{h-\frac{d}{2}}{\sqrt{2}\sigma_1}\right)}{erf\left(\frac{d}{2\sqrt{2}\sigma_1}\right)}\right] \quad (6.27)$$

This relation was plotted as a function of detector spacing h (see Figure 6.11). For example, if the requirement is for -60 dB electrical crosstalk, a spacing h = 420 µm is necessary, corresponding to an angular spacing

$$\varepsilon = \frac{h}{f} = \frac{420.10^{-6}}{26.10^{-3}} = 16.15\ .10^{-3}\ \text{rad} = 0.92°$$

Thus, with the limitation 3° off-axis, the usable field angle (both sides) is 6°. We can expect to have approximately N channels, where

$$N = \frac{6°}{0.92°} = 7\ \text{channels}$$

6.4.7 Example of Possible Implementation

The 7 channels are equally spaced in the detector plane (this is not strictly exact, because dispersivity 6.5 is not constant over the range 800-900 nm; but the error in this approximation is less than 1%, and will not affect the value of N).

Location of the 7 detector centers along y_d:

-1260 -840 -420 0 420 840 1260 yd(µm)

The corresponding LD center-wavelengths are derived from 6.6, which shows that one needs a dispersivity

$$D_a/850\ \text{nm} = 8.56 \times 10^{-4}\ \text{rad/nm}$$

So, the LD's will be separated in wavelength by

$$\frac{\varepsilon}{D_a} = \frac{16.5\ .10^{-3}}{8.56\ .10^{-4}} = 18.9\ \text{nm}$$

To summarize the results, Table 6.1 shows the LD center-wavelengths, and the corresponding angular and spatial positions of the detectors.

6.5 OTHER CONSIDERATIONS

Before manufacturing such a WDM DEMUX, it will be necessary to deal with various considerations, such as:

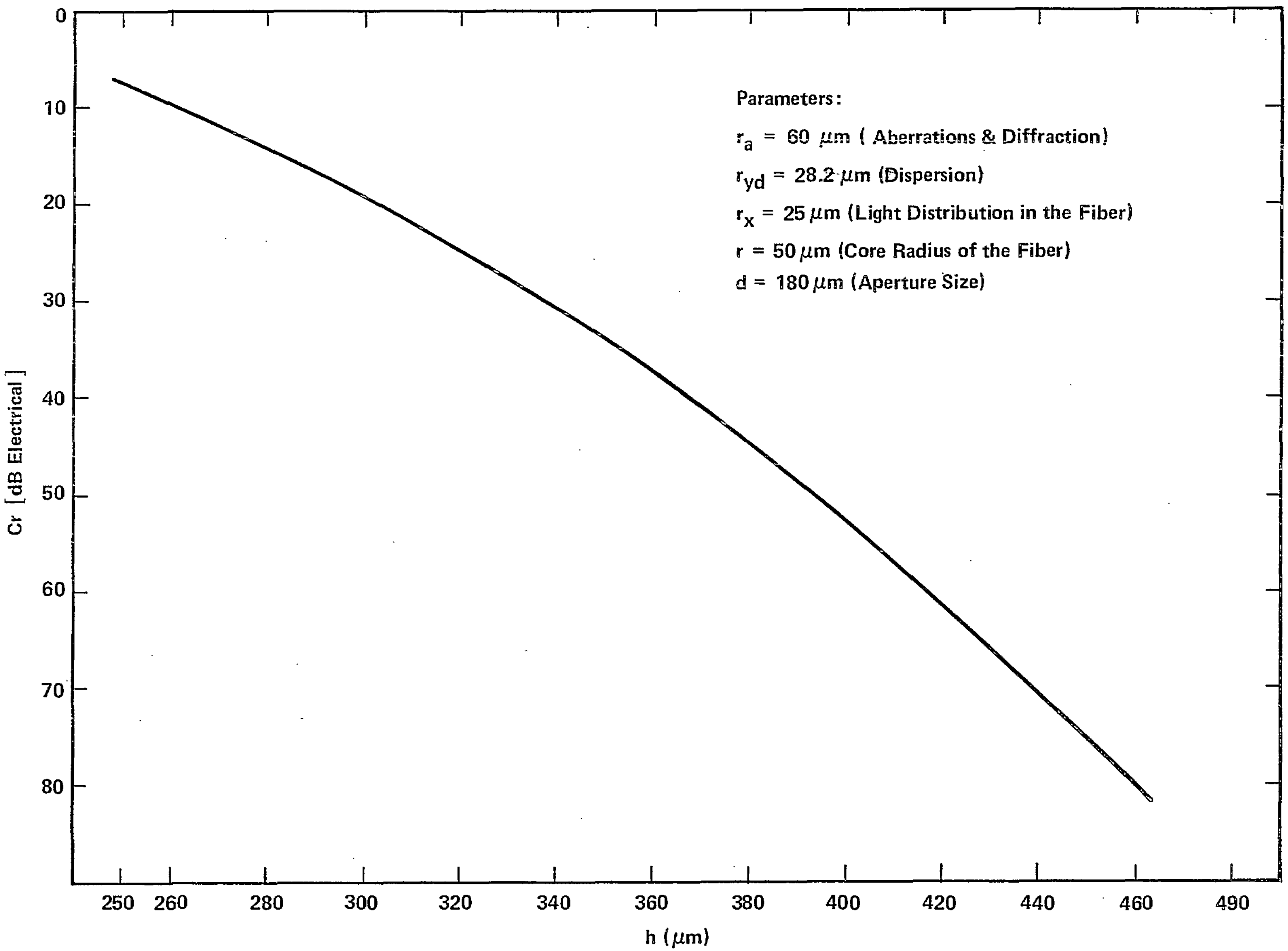

Figure 6.11 Crosstalk as a Function of Detector Spacing

TABLE 6.1. Parameters Describing Each of the 7 Channels

Channel no.	1	2	3	4	5	6	7
LD center wavelength λ_i [nm]	793.4	812.2	831.1	850	868.9	887.8	906.6
Diffraction angle, θ_2, at λ_i	17.2°	18.2°	19.1°	20°	20.9°	21.8°	22.8°
Detector location y_i [μm] along y_d	-1260	-840	-420	0	420	840	1260

- Grating imperfections. Depending on the precision of the ruling machine, spurious light is reflected from a grating ("ghosts" and scattered light). But near autocollimation, references 6.2 and 6.6 state that this light is typically 0.01% to 0.001% of the incident light. So, the added crosstalk remains small-between 80 and 100 dB down.

- Lens reflectance. Though it influences insertion loss, the more serious effect of lens reflectance is its contribution to crosstalk. Indeed, each face of the lens reflects a part of the incident light in various directions, producing crosstalk between all channels. But with appropriate multilayer coatings, references 6.7 and 6.4 mention the reflectance may be reduced to a very low value in a specific wavelength range, although no more precise figures are given.

- LD characteristics. Drift (due to temperature) and spreading of the emission spectrum (due to ageing) can greatly affect the performance of a WDM system.

- Mechanical constraints. Because of the small size of the optical images, tolerances on locating fiber and detectors are quite severe. Misalignments could severely reduce the device performance.

6.6 CONCLUSIONS

It follows from the work in this chapter that the performance required in a WDM demultiplexer can easily be achieved with diffraction gratings and lenses which are commercially available. The number of channels resolvable by the demultiplexer could be increased significantly if light sources in the 1.05 to 1.3 μm region were used together with sources in the 800 to 900 nm range.

6.7 REFERENCES

6.1 James E. Stewart
"Infrared Spectroscopy" chapt. 5.5
Dekker, Inc. New-York 1970

6.2 Jobin-Yvon Optical Systems
"Handbook of Diffraction Gratings: Ruled and Holographic"

6.3 Joseph W. Goodman
"Introduction to Fourier Optics" chapt. 2
Mc. Graw-Hill, 1968

6.4 Melles Griot
"Optics guide" (1975)

6.5 E.G. Loewen, M. Nevière, D. Maystre
"Grating efficiency theory as it applies to blazed and holographic gratings"
Applied Optics - October 1977.

6.6 PTR Optics Corp.
"Diffraction grating catalog"

6.7 K. Rabinovitch and A. Pagis
"Multilayer antireflection coatings: theoretical model and design parameters"
Applied Optics - June 1975.

6.8 M. Born and E. Wolf
"Principles of Optics"